# NUMERICAL MODELLING OF THE PROPAGATION ENVIRONMENT IN THE ATMOSPHERIC BOUNDARY LAYER OF LITTORAL AREAS

Initial Conditions in the Mesoscale Model

R. S. Plant and B. W. Atkinson

Department of Geography
Queen Mary and Westfield College
University of London

Phase 2 - Report No 4
MoD Agreement No. FS2/2042/02

July 2000

# Contents

## Abstract

Previous reports from this project have described mesoscale–model simulations of the refractivity environment over the Persian Gulf on the occasions of research flights in that area. The simulations captured the development of stable marine internal boundary layers (MIBLs), resulting from the flow of hot, dry air from Saudi Arabia over the waters of the Gulf. Because it is also forced by land–sea contrasts, a sea-breeze circulation frequently occurs in association with the MIBL. The size, location and internal structure of the sea-breeze circulation were also realistically simulated.

The initial conditions used in previous simulations were somewhat idealized. In this report some of the initial profiles used are set directly from real data. Four sets of simulations are described, with initial conditions of varying degrees of idealization. All of the sets produced results in broad agreement with observations taken in the SHAREM-115 programme. Because of the strong forcing mechanism of the diurnal cycle, the overland results are insensitive to the starting conditions. Reasonable qualitative results over the Gulf waters are obtained from a crude initialization of the model in which a single land–based sounding provides the starting conditions throughout the model domain. This indicates that the model itself has predictive power. However, detailed quantitative prediction of the propagation environment does require good initial data on the low-level atmospheric conditions over the Gulf. Incorporation of such data yields dramatic improvements to the predictions. In practical forecasting it may be far more valuable to obtain limited data for the low-level conditions over the sea than to assimilate large amounts of overland synoptic data.

# 1 Introduction

This project is concerned with assessing the capability of mesoscale numerical models for predicting the propagation environment in coastal areas. Phase 1 covered the testing of a non-hydrostatic, numerical model in idealised and realistic situations (Li and Atkinson, 1997a,b, 1998a,b). The realistic cases (Li and Atkinson, 1998b) were run to simulate conditions in the Persian Gulf in a period when aircraft observations had been taken (Brooks *et al.*, 1997, 1999). The results were encouraging and showed that the model was capable of capturing the essential features of the propagation environment. A marine boundary layer (MBL) over the Gulf was well simulated in both its depth and the gradients of temperature, humidity and refractivity therein. In addition to the important vertical gradients at the top of the MBL, well-developed sea-breeze circulations were found which exhibited a strong horizontal gradient at the boundary between sea and land air. It is tempting to call this gradient the sea-breeze front (SBF), but care in nomenclature is required here as observations of such fronts show them to be hundreds of metres, rather than several kilometres, wide.

In the light of the results from Phase 1 it was decided to pursue four aspects of the project: first, the effects of horizontal grid resolution on the simulations; second, a more detailed analysis of the SBF; third, horizontal variations within the MBL; fourth, the incorporation of the `TERPEM` model, a code that allows calculation of the response of electromagnetic radiation to the refractivity environment produced by the meteorological model. Plant and Atkinson (1999, 2000a,b) have discussed the effects of grid resolution (1999), the development of the marine internal boundary layer (2000a) and the application of `TERPEM` (2000b).

Previous work on this project has employed somewhat idealized initial conditions in the mesoscale model. In this report we consider the effects of setting the initial conditions directly from real data. This is clearly an important issue if a mesoscale model is to be used as part of a practical forecast of the propagation environment. It should be noted that a similar discussion of this problem has been presented by Atkinson *et al.* (2000). However, we feel that it may be useful to offer a somewhat more detailed discussion here, tailored to the specific context of the project. Since we have speculated on several occasions that inhomogeneities of the sea surface temperature (SST) may be significant (Li and Atkinson, 1998b; Plant and Atkinson, 2000a) we also describe some model runs in which artificial, but realistic, SST variations have been imposed for illustrative purposes.

## 2 Prediction of the Refractivity Environment

Within a given refractivity field the propagation of radar signals can be modelled with good accuracy using parabolic equation models (Dockery, 1988; Craig, 1988; Dockery and Goldhirsh, 1995). A detailed example of the application of such a model was given by Plant and Atkinson (2000b). In practice the most difficult aspect of predicting the propagation environment is the prediction of the refractivity field. This view was recently stressed by Christophe *et al.* (1995) who argued that obtaining meteorological profiles is currently a more important task than assessing them in radar models. Observational data providing refractivity profiles tends to be infrequent (routine observations are typically made at 12 hr intervals) and widely spaced. The sparsity of data is especially a problem over the sea since a refractivity profile can normally be measured only at a particular location if there happens to be ship at the point. Although observational flights can be made and have yielded valuable, high–quality datasets, this approach is impractical for routine data gathering. Work is continuing in order to ascertain the acceptable space and time separations in recorded data that are required for useful prediction of the propagation environment (see, for example, Dockery and Goldhirsh (1995); Rogers (1995); Brooks *et al.* (1999)).

A particularly useful phenomenon to be able to predict would be that of radar ducting (Turton *et al.*, 1988). This refers to strong trapping of radar signals, concentrating the radar energy within some limited vertical range (the duct) and producingly correspondingly weak signals outside of that range. There are several types of meteorological conditions that can lead to duct formation (Skolink, 1980; Turton *et al.*, 1988), one of which is the advection of warm, dry continental air over a cooler sea. When the warm air from a dry landmass moves over the cooler sea water, the lowest layers of the air are cooled and moistened within a stable internal boundary layer (IBL) (Garratt, 1990). As this IBL forms over water it is called a marine internal boundary layer (MIBL). The moisture accumulated in the stable surface layer is a major cause of an increase in radar refractive index with height and the formation of a radar duct with a depth approximately equal to that of the MIBL. This effect may reinforce a pre-existing evaporation duct and so increase its depth. Advection ducts are also sometimes observed when warm moist air is advected over a cooler sea, resulting in the formation of sea fog with a duct near the top of the fog.

The advection duct is by no means uncommon in littoral regions and can significantly affect radar communications between land and sea stations. Being closely associated with the MIBL the duct properties can vary quite considerably with fetch and this variation must also be captured in the refractivity dataset if the propagation is to be accurately modelled. Moreover, the MIBL is strongly dependent on the land–sea temperature difference and thus the ducting conditions can undergo important changes in the course

of a few hours. It is therefore clear that observational programmes as currently envisaged are unable to provide direct refractivity input to propagation models of sufficient quality for realistic prediction of important effects within littoral regions.

An attractive alternative is the use of a mesoscale numerical model. The hope is that one can initialize such a model using a fairly sparse dataset and then use the model output to produce refractivity profiles which evolve in a realistic fashion with changes in location and time. Several mesoscale models have already been investigated in this context. Lystad and Tjelta (1995) simulated the refractivity field over a coastal area of Norway at about 65°N. On comparison with radiosonde measurements, their model proved useful in predicting the spatial distributions and diurnal variations of refractivity, but it missed the fine vertical structures that are also of critical importance for radio propagation. Burk and Thompson (1995, 1997) modelled the summertime refractive conditions in the southern California Bight, using the Navy Operational Regional Atmospheric Prediction System (NORAPS). The hydrostatic, regional model was nested in the Navy's global model, which provided time-dependent lateral boundary conditions for the regional model. Despite the coarse horizontal resolution (20 km), a simulated sea–land breeze was generally in agreement with coastal station observations. Model simulation showed significant diurnal variations in the MBL along the central coastal portion of the southern California Bight but such variations diminished rapidly away from the coast.

Studies such as those above have provided grounds for optimism regarding the use of a refractivity field produced from a mesoscale model as input to radar propagation models for forecasting the propagation environment. This project has used the UK Met. Office mesoscale model (Ballard and Golding, 1991) to simulate the refractivity environment in the Persian Gulf on the occasions of research flights in that area. Observations were taken by the UK Met. Office C-130 Hercules aircraft during the SHAREM-115 exercise in April 1996 (Brooks *et al.*, 1997, 1999; Brooks and Rogers, 2000). The five research flights may conveniently be split into two groups according to the boundary layer conditions. Flights on the 23 rd and 25 th April were characterized by relatively low wind speeds ('low-wind' cases), typically from 5 to 10 $\mathrm{ms}^{-1}$, and an inversion of height 100 m or less. Flights on the 27 th, 28 th and 29 th April were characterized by higher wind speeds (hereafter known as 'high-wind' cases) of up to about 23 $\mathrm{ms}^{-1}$, and a deeper surface layer with an inversion at $\sim 300$ m. The same split has been followed in the simulations, which have successfully captured important features of the littoral propagation environment (Li and Atkinson, 1998b; Plant and Atkinson, 2000a,b).

The studies performed by Lystad and Tjelta (1995) and Burk and Thompson (1995, 1997) used mesoscale numerical models which were nested within synoptic–scale models. In both cases the synoptic model was initialized in

a forecasting mode with full data assimilation of routine synoptic observations. Results from the synoptic model were then used to provide initial and boundary conditions for the mesoscale model. By contrast, in this project a mesoscale model has been used as a stand–alone code, with somewhat–idealized initial conditions that are based on the aircraft observations of Brooks *et al.* (1997, 1999). This has allowed us to examine the capability of the model to capture the essentials of the boundary layer and duct conditions in the Gulf area. However, in a routine prediction of advection ducting high–quality initial conditions of that sort would not be available. Here we wish to test the use of synoptic–scale data as input to the model.

Four sets of numerical experiments are compared. Each set comprises low-wind and high-wind cases in north–westerly airflow from the land to the west of the Persian Gulf. In both cases the wind profiles are smoothed composites of a sounding at Kuwait International Airport (KIA) (KIA data, 1996) and the winds observed by the ship US Caron and by the aircraft in SHAREM-115 (Brooks *et al.*, 1997). These profiles are used in all the sets. The first set (Set 1) uses idealized but realistic profiles of temperature and humidity and was reported by Li and Atkinson (1998b). The second (Set 2) uses particular radiosonde ascents from KIA to initialize the model and the third (Set 3) uses combinations of particular radiosonde ascents and the SHAREM-115 data for initialization.

A fourth set (Set 4) uses idealized initial conditions similar to those of Set 1. However, in this set the SST is allowed to vary with position. As noted above, this project has studied the formation of a marine boundary layer as a warm, dry air mass is advected by the synoptic wind from the deserts of Saudi Arabia across the waters of the Persian Gulf. The process is sensitive to the temperature difference between the sea surface and the overlying air and thus to the SST itself. For example, it was noted by Plant and Atkinson (1999) that an increase of the SST from 23°C to 24°C produced a slightly shallower MBL. It is therefore interesting to investigate the effects of spatial variations in the model SST.

# 3 Initial Conditions

The model domain is chosen to cover the central part of the Persian Gulf (Figs. 1 and 2), where aircraft observations were made in 1996 (Brooks *et al.*, 1997, 1999; Brooks and Rogers, 2000). For the first three sets, the horizontal domain has a grid length of 6 km over an area of size $600 \times 360$ km centred at 51°E, 27°N. There are 33 levels specified in the vertical, extending up to 10 km above the surface and with a level spacing that increases with height in order to obtain good resolution at low altitudes.

As in Li and Atkinson (1998b), wind profiles are set at intermediate heights from the synoptic conditions, and fall off linearly towards zero in the

top few levels of the model and logarithmically towards the surface. The fall off at large heights is clearly artificial and is imposed for consistency with the simple boundary conditions used, which are essentially those of a rigid top where variables remain fixed at their initial values. Test runs have confirmed that these top boundary conditions are adequate for our present purposes since the top few levels of the model are almost static, the thermally–induced coastal circulations having a depth less than $\sim 3$ km. The winds are introduced by specifying the normal components of velocity on the lateral boundaries.

In the low-wind case the winds at intermediate levels are set as $u = 3, v = -4\,\mathrm{ms}^{-1}$ whilst the high–wind case uses $u = 12, v = -9\,\mathrm{ms}^{-1}$. These choices are based on the data presented in Figs. 3 and 4 of Brooks *et al.* (1997) between $\sim$ 200 and 1000 m. The figures show synoptic soundings from KIA at 1200UTC and aircraft observations at roughly similar times[1]. From Fig. 1 it can be seen that KIA lies $\sim 100$ km upstream of the model domain, and thus data recorded there is less likely to be characteristic of Gulf conditions than data taken over the Gulf itself. The KIA data (1996) gives wind speeds of $\sim 10\,\mathrm{ms}^{-1}$ in both high- and low-wind cases and only distinguishes between them through the wind direction, which agrees with that from the aircraft in the high-wind case but which is northerly rather than north–westerly in the low-wind case. In addition, in the high-wind case there is also available a rawinsonde sounding, made at 1330UTC from the ship USS Caron within the Gulf (Fig. 4 of Brooks *et al.* (1997)). The rawinsonde data is undeniably in closer agreement with the aircraft profile than the KIA profile. There is insufficient data available to allow the wind profiles used in the mesoscale model to vary with time or position in any meaningful way and thus it is important to choose profiles that are consistent with those observed by SHAREM-115 over the Gulf during the afternoon. We therefore regard the aircraft observations at $\sim$1200UTC as the appropriate data sources for model winds. Above the lowest hundred metres or so, there is little variation in the winds with height, justifying our decision to neglect such variations.

The other initial conditions required in the mesoscale model runs are the sea-surface temperature (SST) and the initial vertical profiles of potential temperature and relative humidity. These conditions vary between the different data sets considered. Note that for a given profile of temperature or potential temperature, an initial pressure field is set from the hydrostatic approximation, applying the method of Li and Atkinson (1997b).

[1]The aircraft data were taken at 1246UTC on the low-wind day and at 1001UTC on the high-wind day.

### 3.1 Set 1 Initial Conditions

For Set 1 idealized initial conditions were chosen (Li and Atkinson, 1998b). By both design and necessity the profiles did not describe conditions at one place at a particular time, but were representative of atmospheric conditions over the Gulf at the time of the SHAREM-115 flights. Horizontally homogeneous conditions were set throughout the model domain and the same conditions were used in both high- and low-wind cases. Runs were initialized at 0700 Local Time (LT), a time for which SHAREM-115 data were available (Brooks *et al.*, 1997), and also a time of day when land–sea thermal contrasts are usually quite small. The actual profiles used were given by Li and Atkinson (1998b) and are simple two-piece functions of height. They are plotted here as Fig. 3 for ease of comparison with the profiles used in the other data Sets.

The sea-surface temperatures used in the Set 1 runs were taken from Figs. 3 and 4 of Brooks *et al.* (1997) — 23°C in the low-wind case and 24°C in the high-wind case.

### 3.2 Set 2 Initial Conditions

In these experiments the initial conditions are set from particular radiosonde ascents at KIA (KIA data, 1996). Such conditions describe the upstream, overland atmosphere, in marked contrast to the initial conditions of Set 1 which represent the downstream, marine atmosphere. Thus the Set 2 configurations contain no information on the marine boundary layer. Any MBL observed within the results could therefore only arise through the action of processes included in the mesoscale model.

Synoptic upper-air observations from KIA are available at 0000UTC and 1200UTC each day. We use data from the 0000UTC soundings on the 23 rd and 28 th April in order to set the low- and high-wind model profiles respectively. This corresponds to 0300LT and therefore the model runs were started at this time. The KIA data (1996) includes values of temperature and relative humidity for a series of heights. These 'heights' are given relative to sea level, the station itself being 55 m above sea level. Since the effects of orography are neglected in the model simulations (see Li and Atkinson (1998b) for the justification), we translate the heights in the KIA data into vertical distances above the surface. At each model level the initial temperature and relative humidity are defined by a linear interpolation between the adjacent KIA data values. Plots of the initial profiles used in Set 2 are given in Fig. 4.

(Temperature information is available from the KIA data (1996) for heights extending above the vertical extent of the model grid. For the realtive humidity, however, the highest data point lies just a few hundred metres below the model top at 10 km. In order to extrapolate up to the model top

we have assumed that the relative humidity falls off at 1 %km$^{-1}$, the same rate as is used for the upper-air conditions of Set 1.)

The Set 1 runs were performed by Li and Atkinson (1998b) prior to publication of the paper by Brooks *et al.* (1999) and therefore these runs used the only values that were available for the SST at that time, taken from Brooks *et al.* (1997). Values given by Brooks *et al.* (1997) refer to the "potential sea surface temperature in the vicinity of [an] aircraft profile". They were obtained from infrared radiometer measurements on the aircraft. In 1999 however, Brooks *et al.* also mentioned SST measurements made on the USS Caron. It is not clear whether or not the ship measurements were used in arriving at the SST values that were quoted for each day in Table 2 of Brooks *et al.* (1999). Nonetheless, since the values in that Table are described as "means for 30-m flight legs" we are inclined to regard them as being more reliable than the values denoted around the position of a single vertical profile in Brooks *et al.* (1997). In the Set 2 runs we have therefore used the SST given by Brooks *et al.* (1999) for the days corresponding to the KIA soundings that supplied the initial vertical profiles. Thus, the SST is taken to be 26.15°C in the low-wind case (23 rd April) and 23.95°C in the high-wind case (28 th April).

### 3.3 Set 3 Initial Conditions

In the idealized Set 1 no distinction was made between the initial profiles over land and sea. In Set 2 a limited degree of land–sea contrast was recognized by the use of (slightly) different values for the SST and the initial land temperature. For the third Set of runs, the initial state of the land boundary layer is derived from the KIA soundings and KIA synoptic observations, similarly to Set 2. However, the initial state of the marine boundary layer is determined from SHAREM-115 observations (Brooks *et al.*, 1997). Set 3 runs are initialized at 0700LT, a time for which SHAREM-115 data are available. The aim is to predict conditions for the following afternoon. Unfortunately, only one set of 0700LT data, taken on a high-wind day, is available from SHAREM-115. In the absence of other appropriate data these are used in both the low- and high-wind runs.

Plots of the initial profiles used over land and sea can be seen in Figs. 5 and 6.

#### 3.3.1 Low Wind Case

Over land we mainly use the KIA sounding from 0000UTC on 23 rd April. Although this was taken four hours before the start of the run, comparison of the 0000 and 1200UTC soundings reveals very small differences in temperature and humidity above a height of 1000 m. Within the lowest couple of hundred metres we prefer to describe the surface conditions by interpo-

lating between the three–hourly KIA synoptic surface observations. Thus, unlike in Set 2 the surface data point from the 0000UTC sounding is discarded. Between the surface and next data point in the sounding (186 m above ground) a linear interpolation is made.

Over the sea, between 30 m and 1000 m, we use the SHAREM-115 temperature data presented in Fig. 23 of Brooks *et al.* (1997). These data were measured over the Gulf at about 0700LT on 28 th April. Between 30 m and the surface, linear interpolation is made to the sea-surface temperature, which is chosen as in the runs of Set 2. For the relative humidity, data from Fig. 23 of Brooks *et al.* (1997) is again used, having made the necessary conversions from humidity mixing ratios. At the surface, a mixing ratio of $10.5\,\mathrm{g\,kg^{-1}}$ is taken, based on an extrapolation of the SHAREM-115 profile. Above 1000 m, the initial conditions over the sea are taken to be identical to those over land. The matching of both variables around 1000 m is good, so that no smoothing between the two data sources is required.

### 3.3.2 High Wind Case

In this case the KIA sounding used for overland grid points is that at 0000UTC on 28 th April. As in the low wind case, comparison of the 0000 and 1200UTC soundings reveals very small differences in temperature and humidity above 1000 m. The surface data point from the sounding is again discarded, together with two near-surface data points at 53 m and 74 m. These are replaced by surface data interpolated from the KIA synoptic observations. Between the surface and the next data point in the sounding, at 193 m, linear interpolation is used.

Over the sea, conditions between 30 m and 1000 m are taken from Fig. 23 of Brooks *et al.* (1997). Matching of the relative humidity to the data from the KIA sounding around 1000 m is again good. However, there is a significant discrepancy between the two data sources with regard to the temperature at this height. In order to obtain a reasonable profile for the initial temperature over the sea, without introducing an artifical inversion above 1000 m, we have performed a linear interpolation between the SHAREM-115 temperature at 1000 m and the data point at 2903 m in the KIA sounding.

### 3.3.3 Horizontal Smoothing

There is a potential for numerical problems in the Set 3 runs owing to the large horizontal gradients in the initial conditions across the coast. In an attempt to avoid such problems we have therefore decided to smooth the initial profiles close to the coast. A simple scheme has been devised whereby for each grid point we draw a $42 \times 42$ km box centered at the point. A factor

$f$, representing the nature of the surface within that locality, is defined by:

$$f = \frac{\text{number of grid points in the box that lie over the sea}}{\text{number of grid points in the box}}. \qquad (1)$$

At intermediate heights, the initial conditions at the point may then be taken to be: $f \times$ (sea conditions) $+ (1 - f) \times$ (land conditions). However, it would not be appropriate to smooth the surface temperature in this fashion, since a step change in surface conditions at the coast is a genuine physical feature. Thus, we also apply an exponential factor so that while the effect of, say, land conditions on a point just out to sea is certainly noticeable above 100 m or so, there is a negligible effect close to the surface. The smoothing used is then:

$$C = gS + (1 - g)L \qquad (2)$$

where $C$ denotes the conditions at the point of interest, $L$ denotes the land conditions, $S$ the sea conditions and $g$ depends on whether the point of interest is over land or sea:

$$g_{\text{land}} = f(1 - \exp(-z/v)); \qquad (3)$$

$$g_{\text{sea}} = 1 - (1 - f)(1 - \exp(-z/v)). \qquad (4)$$

The constant $v$ has been set at 50 m.

### 3.4 Set 4 Initial Conditions

For all of the model simulations reported so far in the project, the sea-surface temperature has been held fixed over space and time. The SST will change only very slowly in time (Reed and Lewis, 1980, and references therein) and this effect can safely be neglected in comparison with uncertainties associated with the amplitude and timing of the diurnal cycle (issues such as the pecise value of the surface albedo and the possibility of cloud formation would appear to be more significant than detailed modelling of the SST time evolution). However, spatial variations across the model domain of the order of a degree or two would certainly not be implausible and may have a noticeable impact on the horizontal variations of the MIBL (see, for example, Clancy *et al.* (1979); Mizzi and Pielke (1984)). In the Set 4 runs the SST is kept constant over time but varies with position. Similar approaches have been followed by Koračin and Rogers (1990); Wai (1988); Wai and Stage (1989) in which it has been shown that sudden changes in the SST can give rise to localized circulations and thermal IBL formation.

Wai (1988) mentions aircraft observations that were made of a localized cold spot in the SST. These observations inspired a mesoscale simulation in which a sinusoidally–shaped dip in SST was considered, a change of 1.7°C

occurring over a distance of 60 km. Variations on the same scale and of the same magnitude are investigated here. Specifically, we use:

$$T = \overline{T} + \frac{\Delta T}{2} \sin\left(\frac{2\pi r}{L}\right) \tag{5}$$

where $\overline{T}$ is the mean SST (taken from Brooks *et al.* (1999) as in Sets 2 and 3), $\Delta T = 1.7°\mathrm{C}$, $L = 120\,\mathrm{km}$ and $r$ is the distance from the NW corner of the model grid. The runs are performed on the cut-down grid used for the run with a 3 km grid length in Plant and Atkinson (2000a). The smaller grid length for this Set is preferred because the effects of the SST variations are most likely to be manifest at short horizontal scales. Initial conditions other than the SST are idealized. They are identical to those described in Plant and Atkinson (1999) (once the appropriate translations have been made to allow for the different SSTs) and so are very similar to those of Set 1. The SST used along the line $y = -54\,\mathrm{km}$ is shown in Fig. 7 for the low wind case.

# 4 Results

## 4.1 Set 1 Results

The results obtained using the idealized initial conditions of Set 1 were discussed by Li and Atkinson (1998b). Some additional discussion of particular aspects of the model results has been given by Plant and Atkinson (1999, 2000a,b). Therefore it is sufficient in the present report merely to recall some general features of the results, for ease of comparison with those of the other Sets. Comparison of the results from Set 1 with SHAREM-115 observations was generally encouraging (Li and Atkinson, 1998b). The juxtaposition of hot, dry land with water in the Gulf region produces strong contrasts between the land and marine boundary layers. In such situations air flowing from the land to the sea is substantially cooled, stabilised and moistened as a MIBL forms over the water surface (Garratt, 1990; Rogers *et al.*, 1995). Despite the horizontally–homogeneous initial conditions the model clearly distinguished the boundary layers over land and water. Over the Gulf the boundary layer was significantly cooler and moister than the equivalent over land and the shape of the potential–temperature profile indicated the cause as cooling by turbulent transfer (Plant and Atkinson, 2000a). In addition, the model distinguished the different depths of the MIBL and associated ducts in the low and high–wind cases, as found in the SHAREM-115 programme.

### 4.1.1 Low Wind Case

Over the land area in the mid-afternoon, a mixed boundary layer about 1 km deep with potential temperatures of $\sim 34°\mathrm{C}$ (Fig. 8a) is associated

with vertically–uniform mixing ratios of $\sim 6\,\mathrm{g\,kg^{-1}}$ (Fig. 8b) and a linearly–increasing modified refractivity (Fig. 8c). In contrast, the lowest 300 m over the sea shows a temperature inversion of $\sim 8^{\circ}\mathrm{C}$ (Fig. 8a), a moistening of the air near the surface with mixing ratios reaching $\sim 16\,\mathrm{g\,kg^{-1}}$ (Fig. 8b) and a lapse of refractivity (Fig. 8c).

Fig. 9 shows the development of the boundary layer in the profiles of potential temperature, mixing ratio and refractivity at the point $x = 210, y = -78\,\mathrm{km}$ far out to sea. By mid-afternoon the isentropic layer is $\sim 100\,\mathrm{m}$ deep and the capping inversion is strengthened to about $0.1^{\circ}\mathrm{Cm^{-1}}$ between 100 and 140 m. Evolution of the water vapour profiles at the same sea point (Fig. 9b) shows that a nearly–constant mixing ratio is maintained in the marine surface layer. Above about 150 m the simulation indicates dry air, possibly due to subsidence associated with the seaward part of the sea-breeze circulation (SBC). The simulated profiles of refractivity (Fig. 9c) show a simple surface duct about 100 to 160 m deep (see also Plant and Atkinson (2000b)), similar to the observed surface duct on 23 rd April (Brooks *et al.*, 1999).

#### 4.1.2 High Wind Case

In the high–wind simulation the marine profile of potential temperature in Fig. 10a reveals the development by midday of a MIBL about 200 m deep overlain by a sharp inversion. The stable layer is about twice as deep as that formed in the low-wind case. The simulated moist near-surface layer (Fig. 10b) is also about 200 m deep and is overlain by air with with a humidity of $\sim 3\,\mathrm{g\,kg^{-1}}$. In the refractivity profile (Fig. 10c), an S-shaped surface duct is evident, in which the trapping and ducting layers are about 100 m and 300 m in depth respectively (Plant and Atkinson, 2000b). Near to the shoreline a simple surface duct occurs in the evolving MIBL, while the S-shaped duct becomes apparent beyond a fetch of about 100 km. The transition between the two types of duct has significant effects on propagation (Plant and Atkinson, 2000b).

### 4.2 Set 2 Results

The Set 2 runs use horizontally–homogeneous initial conditions derived from the overland sounding at KIA. Not surprisingly, the humidity at low altitudes is significantly lower than in the initial conditions of Set 1 (see Figs. 3 and 4). In the Set 2 model runs, evaporation causes the humidity over the sea to increase towards more realistic values. Several hours of model time are required for a reasonable degree of adjustment.

The land–sea contrast is weaker in the Set 2 runs than in the runs of Set 1. In the low-wind case this occurs because of the increased SST (Sec. 3.2). A similar effect in the high-wind case may be related to the low overland

temperature at the start of the model run (Fig. 4). In this case the overland heating seems to be somewhat underestimated and so conditions overland remain quite cool compared to the runs with other initial conditions. The loss of land–sea contrast may partially explain why the MIBL is altogether a rather weaker structure in the Set 2 runs.

### 4.2.1 Low Wind Case

Fig. 11 shows profiles of simulated potential temperature, mixing ratio and refractivity, together with observed values (Brooks *et al.*, 1997) at the point $x = 210, y = -78\,\mathrm{km}$ in the early afternoon. A mixed layer develops of $\sim 300\,\mathrm{m}$ depth with a potential temperature of about $25.5^\circ\mathrm{C}$ (Fig. 11a), roughly equal to the SST used in the run (Sec. 3.2). This mixed boundary layer is capped by an inversion with a potential temperature difference across it of only $\sim 2^\circ\mathrm{C}$. Potential temperatures in the lowest 70 m compare well with observed values, but above that height the simulated values are much lower than those observed. Thus, the modelled thermal boundary layer is too deep and too cold.

Associated with the mixed thermal layer a moist, marine boundary layer exists below $\sim 300\,\mathrm{m}$ (Fig. 11b). It is about three times deeper than that observed and the near–surface magnitudes are underestimated by $\sim 6\,\mathrm{g\,kg^{-1}}$. Examination of the areas beneath the curves on Fig. 11b suggests that the model managed to capture quite well the evaporation from the surface, so that the total amount of water vapour within the MIBL was correctly predicted. However, the vapour is mixed through a deeper layer than occurred in nature. A refractivity profile exhibiting surface ducting is produced below 300 m, a height slightly more than twice that observed. This occurs because the refractivity profile follows that of humidity to large degree, leading to under–prediction of the modified refractivity below about 100 m and over–prediction above that height.

### 4.2.2 High Wind Case

Simulated and observed (Brooks *et al.*, 1997) profiles for the high-wind case are shown in Fig. 12 for the point $x = 186, y = -54\,\mathrm{km}$ in the early afternoon. The potential temperature in the mixed layer is about $24^\circ\mathrm{C}$, in accordance with the SST. The boundary layer generated in the run is about 600 m deep, capped by a weak inversion. Observations reveal (Fig. 12a) that the simulated temperatures are correct in the lowest 200 m of the boundary layer but that the height and strength of the capping inversion are, respectively, too large and too small. The simulated magnitudes of humidity below about 200 m are in reasonable agreement with observations (Fig. 12b), but the sharp lapse between $\sim 200$ and 550 m is not captured in the simulations. As the refractivity is strongly dependent on the humidity its profile also does

not display the strong lapse above 200 m, but the magnitudes below that height are captured in the simulation. A trapping layer is found between 500 and 600 m, giving rise to a weak elevated duct between 400 and 600 m, in contrast to the observed surface duct below $\sim 270$ m (Brooks *et al.*, 1999).

### 4.3 Set 3 Results

The Set 3 runs use different initial conditions over the land and sea surfaces, taking the former from KIA data (1996) and the latter from SHAREM-115 observations. The results are generally good, an IBL of roughly the correct depth being produced. There are strong gradients at the IBL top in the low-wind case, and more modest ones in the high-wind case. These gradients are stronger than those found in Set 2. The model certainly spins-up more quickly than in Set 2, which took some time to settle down and to distinguish between land and sea conditions in a realistic fashion. This provides some indication that the initial conditions of Set 3 may indeed be more appropriate for the situation modelled.

The air at about 500 m over the sea remains very dry through to the early afternoon. This dryness is passed to the model through the Set 3 initial conditions (Figs. 5 and 6). The air at this height is largely decoupled from the direct influence of the sea surface due to the MIBL. Hence, the likely mechanism in the model for moistening of the air at such heights is the movement over the sea of the relatively–moist land air. In that case the specification of the initial humidity profile overland may have an important effect on the humidity of air above the MIBL during the afternoon, and hence also on the strength of the simulated humidity inversion.

#### 4.3.1 Low Wind Case

Fig. 13a compares predicted afternoon profiles of potential temperature with observations from SHAREM-115 at 1415–1425LT on 23 rd April at the point $x = 210, y = -78$ km. A simulated mixed boundary layer, with a depth of 100 to 130 m, is capped by an inversion. Observations showed a mixed layer of about 70 m in depth, overlain by a strong inversion of $\sim 8^{\circ}$C between 130 and 200 m. The predicted humidity profiles (Fig. 13b) show a moist MIBL below $\sim 130$ m with the magnitudes close to the surface being under–predicted. The refractivity profile follows that of humidity quite closely. Although the run under–predicted $M$ magnitudes throughout MIBL, and consequently also the strength of the capping lapse, the surface duct is clearly captured. In view of the fact that the low–level initial conditions for this run were necessarily taken from data on a high-wind day (see Sec. 3.3), the above results are regarded as being broadly successful.

### 4.3.2 High Wind Case

It was noted in Sec. 3.3.2 that specification of the initial temperature profile over the sea requires an interpolation between two data sources from 1000 to $\sim 3000$ m. The importance of ensuring a good match between the sources can be illustrated using a run in which interpolation is made between 1000 and 2000 m. In that case there is an artifical temperature inversion in the initial conditions which causes the model to crash in the early afternoon. Although there is also a crash when interpolation up to $\sim 3000$ m is used, this occurs during the late afternoon. Reasonable results are produced at low altitudes throughout the run, enabling a sensible comparison to be made with the afternoon results from the runs with other data sets.

Fig. 14a shows the profiles of simulated and observed (Brooks *et al.*, 1997) potential temperature in the lowest kilometre of the atmosphere. Up to $\sim 400$ m the simulation results are good, capturing both the cool near-surface layer over the Gulf water and the lower part of the inversion that caps that layer. However, temperatures in the higher levels of the inversion are under–predicted. Whilst the general shape of the humidity profile (Fig. 14b) is reasonable up to $\sim 300$ m the model over–predicts the mixing ratio by $\sim 2\,\mathrm{g\,kg^{-1}}$ at low levels. Between 250 and 550 m, where the air is very dry, the over–prediction increases to $\sim 4\,\mathrm{g\,kg^{-1}}$. A MIBL is produced in the simulation but its predicted top is not as sharply defined as in the observations. Predicted magnitudes of the refractivity above 700 m are in good agreement with the observations. Below that height the magnitudes are too large but the profile shape matches that of the observations quite well. The discrepancy between simulation and observations in this layer is largely determined by the profile of humidity. Despite the discrepancy a surface duct is just discernible and its depth is correctly predicted as 300 m.

## 4.4 Set 4 Results

Results from Set 4 are shown in the form of cross-sections of vapour pressure along the line $y = -54$ km. The atmospheric variations caused by the spatial variations of SST are more pronounced for this variable than for the temperature and the potential temperature (which appears to be little affected). Cross-sections from the low-wind run are given in Fig. 15 whilst results from the high wind run can be seen in Fig. 16. The effects of the varying SST are strongest at the lowest levels and so are rather more evident in the shallow MIBL that develops under low wind conditions.

Interestingly, the region of low SST in the low wind case is associated with an increased vapour pressure, particularly just above the surface. Although the surface flux of humidity will be relatively modest in this region, it appears that a large vapour pressure develops due to the location of the SST minimum relative to the SBC. As shown in Fig. 17, the low-level air

travels only slowly across the minimum which allows for an accumulation of water vapour. A similar, but less pronounced, effect can be seen in Fig. 3 of Plant and Atkinson (1999) which shows cross-sections of vapour pressure from low wind runs with a constant SST. The precise effect in a particular model run will be sensitive to the detailed model description of the SBC. There are some hints in Fig. 15 that a circulation may be developing between regions of warm and cool SST, with strong horizontal gradients of humidity occurring at around $x = 80\,\mathrm{km}$ (note that any such circulation is likely to be weak and so would be difficult to disentagle from the strong SBC in the wind field of Fig. 17). However, this may be a little close to the model boundary for the circulation to have been accurately represented.

Horizontal diffusion is included in the mesoscale model as a mechanism for numerical smoothing (Ballard and Golding, 1991). While valuable in suppressing numerical modes of solution this may also suppress some physical effects. For instance, it will tend to smear–out slowly–varying waves on a scale of a few grid lengths. Thus, the horizontal variations in the model results that can be forced by inhomogeneity of the SST tend to decay as the model run progresses (see Fig. 15) and may be somewhat underestimated. It is clear that realistic variations of the SST can have significant effects on the short–scale horizontal structure of the MIBL and so could have a role to play in accounting for the wavelike features observed by Brooks *et al.* (1997).

If one wished to obtain good representations of these effects it would be necessary to have access to accurate SST data with good horizontal resolution. Some information may be available from satellite observations. In addition, it may be possible to reduce the SST data requirements by coupling the mesoscale atmospheric model to an oceanic model, as described for example by Hodur (1997) for the US Navy's `COAMPS` model. It could also be useful to investigate the horizontal diffusion in the mesoscale model. For example, one might consider the viability of smaller choices for the numerical diffusion coefficients, particularly in the lower part of the model atmosphere. Nonetheless, for a complete description of the short–scale variations seen by Brooks *et al.* (1997) it seems probable that other physical mechanisms would also have to be taken into account. SST variations do not seem to be capable of explaining the observed waves near the top of the MIBL in the cross-sections of potential temperature in the high wind case. Such details could perhaps only be captured with an explicit representation of entrainment in the modelling.

### 4.5 Horizontal Cross Sections from the Set 3 Runs

Observations (Brooks *et al.*, 1997, 1999), and model results from this project, have shown that horizontal variation in the MIBL may have a significant impact on the stucture of the propagation environment. Previous stud-

ies of littoral refractivity environments (Lystad and Tjelta, 1995; Burk and Thompson, 1995, 1997) have had access to verifying data from only a few isolated loactions within the simulated domain. The SHAREM-115 observations, however, are sufficiently detailed that vertical cross-sections can be constructed through horizontal lengths of up to about 100 km (Brooks *et al.*, 1997). During the SHAREM-115 programme data was collected along the lines AB and CD, shown in Fig. 2. Cross-sections of potential temperature and modified refractivity along those lines are compared here with simulation results from the low-wind and high-wind cases of Set 3.

### 4.5.1 Low Wind Case

Figs. 18 and 19 show cross-sections of the simulated and observed potential temperature and refractivity along the line AB in Fig. 2. Appropriate cross-sections were unavailable for 23 rd April and so those for 25 th April, also a low-wind day, are used instead. This, together with the use of high-wind SHAREM-115 data in the initial conditions, means that some discrepancies between simulation and observations are only to be be expected. The distributions of potential temperature (Fig. 18) confirm that the simulated MIBL is deeper than that observed. As the model run progressed the depth of the layer decreased, suggesting that the anomaly introduced in the initial conditions was being rectified by the model processes. In contrast, the intensity of the simulated temperature inversion capping the boundary layer is in good agreement with the observations. The section of simulated refractivity (Fig. 19a) shows the high values seen in the observations (Fig. 19b) at distances up to $\sim 40$ km from point A. Simulated low values beyond 50 km (Fig. 19a) lay at about 250 m, whereas in reality they lay between $\sim 100$ and 200 m. For both variables the observations revealed entrainment and wave-like features in the layer. Neither of these characteristics is captured by the simulation, a point discussed by Plant and Atkinson (2000a) as well as in Sec. 4.4 above.

### 4.5.2 High Wind Case

Figs. 20 and 21 show sections of the simulated and observed potential temperature and refractivity along the line CD in Fig. 2. Comparison of the potential temperature sections (Fig. 20) reveals three main points. First, the model captured the inversion capping the MIBL. Second, the downwind slope of the inversion was modelled. Third, the base of the inversion (shown most clearly by the 25°C isoline) is quite well modelled, but the intensity of the inversion, as noted earlier, is under–predicted. The refractivity is over–predicted by a few percent and its distribution is out of phase with the pattern seen in the observations (Fig. 21). The simulated high values between 200 and 400 m extend too far downwind, displacing the lower values

in the same layer to beyond 80 km. The small–scale structures found in both sets of observations are not captured by the simulation.

# 5 Conclusions

This project is concerned with prediction of the propagation environment over littoral areas, using a mesoscale model to predict the refractivity. It has been fortunate to have the use of high–quality data on the duct environment in the Persian Gulf (Brooks *et al.*, 1997, 1999) but their quantity and distribution in time and space, together with the relative sparsity of routinely available meteorological data, has meant that some idealization has been necessary in choosing initial conditions for the mesoscale model. The present report has described four sets of numerical experiments that were conducted with initial conditions of varying degrees of idealization. All of the sets produced results in broad agreement with the observations taken in the SHAREM-115 programme, but the level of agreement was sensitive to the initial conditions.

The runs performed for a previous report from the project (Li and Atkinson, 1998b) have been referred to here as Set 1. These experiments used idealized initial conditions that characterized the marine atmosphere at the time of the SHAREM-115 research flights. Such conditions are clearly inappropriate for the overland areas of the model domain, but they did provide a good starting point for the atmosphere over the Gulf waters. The experiments tested the feasibility of using a mesoscale model to study the propagation environment in the Gulf. They showed that the model was able to capture successfully the different boundary layers over land and sea and within the latter to distinguish the states formed under low- and high-wind conditions. Given the initial conditions the fact that a MBL was produced of roughly the correct depth hardly represents a triumph for the application of the model. However, the model was able to generate a credible mixed boundary layer overland and to produce conditions over the sea surface that varied with position and time in a realistic fashion. This is illustrated by the production of an internal boundary layer whose depth varied with fetch and by the evolution of a sea-breeze circulation (Li and Atkinson, 1998b; Plant and Atkinson, 1999, 2000a).

Set 2 used less idealized initial conditions obtained from routine upstream, overland soundings (KIA data, 1996). The same conditions were applied throughout the model domain and so no account was taken of the distinctive boundary layer over the sea. This Set therefore provides a useful contrast to the initial conditions of Set 1. An MIBL was succesfully produced in both the high- and low-wind cases. However the depths of the layer were too large and the gradients at the top of the MIBL were under–estimated. The use of a single routine land ascent to initialize the model for

prediction of duct occurrence, depth and strength is clearly very attractive. The results of Set 2 suggest that good, qualitative information could be obtained in this manner, but that for detailed, quantitative prediction such a strategy would be over ambitious.

The experiments in Set 3 relaxed the assumption of horizontal homogeneity in the initial conditions, using different initial profiles over land and sea. SHAREM-115 observations gave a description of atmospheric conditions up to a height of 1 km and this was used for the sea areas in the domain. Above that height data from a routine ascent was used and the same ascent was used to describe conditions over the land areas. The crucial difference from Set 2 is that these runs included a MBL from the outset. The results showed distinct improvements over those from Set 2 and were of a similar level of quality to those from Set 1. The afternoon MIBLs in both high- and low-wind conditions were in closer agreement with observations than the equivalent cases in Set 2. Consequently the model descriptions of the ducts were much improved.

The SHAREM-115 observations revealed variations in the MBL with horizontal scales of the order of a few kilometres or so (Brooks *et al.*, 1997). It has not been possible to capture such variations in the simulations when homogeneous initial conditions are used (Plant and Atkinson, 2000a). In the experiments of Set 4, the sea-surface temperature was allowed to vary with position in an artificial, but realistic fashion. Although the introduction of SST variations did not provide a complete explanation for the short–scale atmospheric variations observed, the results from Set 4 did suggest they may be an important factor. Wavelike fetaures in the MBL were forced by changes in the SST.

In studying the sensitvity of the results to the initial conditions it has been clear that the best results are obtained when the initialization includes data on low-level atmospheric conditions over the Gulf waters. Thus, some knowledge of the near-surface atmosphere over the Gulf appears to be necessary in order to have an opportunity of forecasting the existence, depth and intensity of ducts in that area.

## References


Atkinson, B. W., Li, J.-G. and Plant, R. S. 2000. Numerical Modelling of the Propagation Environment in the Atmospheric Boundary Layer over the Persian Gulf. *revised paper, submitted to J. Appl. Meteorol.*

Ballard, S. P. and Golding, B. W. 1991. *Short Range Forecasting Research, Mesoscale Documentation Paper No. 4 — Basic Model Formulation.* Tech. Rept. Met. Office. documenation paper version 1.5.1, 44pp.

Brooks, I. M. and Rogers, D. P. 2000. Aircraft Observations of the Mean and Turbulent Structure of a Shallow Boundary Layer over the Persian Gulf. *Bound. Lay. Meteorol.*, **95**, 189–210.

Brooks, I. M., Rogers, D. P. and Goroch, A. K. 1997. *SHAREM-115 Observations: Atmospheric Environmental Data Collected by the UK Meteorological Research Flight C-130 Hercules Aircraft.* unpublished report available from ftp://megan.ucsd.edu/pub/sharem, 53pp.

Brooks, I. M., Goroch, A. K. and Rogers, D. P. 1999. Observations of Strong Surface Radar Ducts over the Persian Gulf. *J. Appl. Meterol.*, **38**, 1293–1310.

Burk, S. D. and Thompson, W. T. 1995. Mesoscale Modelling of Refractive Conditions in a Complex Coastal Environment. *In: Propagation Assessment in Coastal Environment.* AGARD Conference Proceedings, vol. 567. Paper 40.

Burk, S. D. and Thompson, W. T. 1997. Mesoscale Modelling of Summertime Refractive Conditions in the Southern California Bight. *J. Appl. Meteorol.*, **36**, 22–31.

Christophe, F., Douchin, N., Hurtaud, Y., Dion, D., Makaruschka, R., Heemskerk, H. and Anderson, K. 1995. Overview of NATO/AC-243/PANEL 3 Activities Concerning Radiowave Propagation in Coastal Environments. *In: Propagation Assessment in Coastal Environment.* AGARD Conference Proceedings, vol. 567. Paper 27.

Clancy, R. M., Thompson, J. D., Hurlburt, H. E. and Lee, J. D. 1979. A Model of Mesoscale Air–Sea Interaction in a Sea-Breeze Coastal Upwelling Regime. *Mon. Wea. Rev.*, **107**, 1476–1505.

Craig, K. H. 1988. Propagation Modelling in the Troposphere: Parabolic Equation Method. *Elec. Lett.*, **24**, 1136–1139.

Dockery, G. D. 1988. Modelling Electromagnetic Wave Propagation in the Troposphere Using the Parabolic Equation. *IEEE Trans. Antenn. Prop.*, **36**, 1464–1470.

Dockery, G. D. and Goldhirsh, J. 1995. Atmospheric Data Resolution Requirements for Propagation Assessment: Case Studies of Range–Dependent Coastal Environments. *In: Propagation Assessment in Coastal Environment.* AGARD Conference Proceedings, vol. 567. Paper 7.

Garratt, J. R. 1990. The Internal Boundary Layer — A Review. *Bound. Lay. Meteorol.*, **50**, 171–203.

Hodur, R. M. 1997. The Naval Research Laboratory's Coupled Ocean/Atmosphere Mesoscale Prediction System (COAMPS). *Mon. Wea. Rev.*, **125**, 1414–1430.

KIA data. 1996. Upper air data from Kuwait International Airport (WMO station 40582) has been obtained for 0000UTC and 1200UTC on 23 rd April 1996 and 28 th April 1996. Surface observations at three–hourly intervals from 0000UTC on these dates were also obtained. These data were kindly supplied to the authors by the UK Met. Office.

Koračin, D. and Rogers, D. P. 1990. Numerical Simulations of the Response of the Marine Atmosphere to Ocean Forcing. *J. Atmos. Sci.*, **47**, 592–611.

Li, J.-G. and Atkinson, B. W. 1997a. *Numerical Modelling of the Propagation Environment in the Atmospheric Boundary Layer Over Coastal Areas: Literature Review and Mesoscale Model.* Tech. Rept. 1. MoD Agreement NNR/2042/1. 36pp.

Li, J.-G. and Atkinson, B. W. 1997b. *Numerical Modelling of the Propagation Environment in the Atmospheric Boundary Layer Over Coastal Areas: Model Sensitivity Study.* Tech. Rept. 2. MoD Agreement NNR/2042/1. 69pp.

Li, J.-G. and Atkinson, B. W. 1998a. *Numerical Modelling of the Propagation Environment in the Atmospheric Boundary Layer Over Coastal Areas: Idealised Case Study.* Tech. Rept. 3. MoD Agreement NNR/2042/1. 65pp.

Li, J.-G. and Atkinson, B. W. 1998b. *Numerical Modelling of the Propagation Environment in the Atmospheric Boundary Layer Over Coastal Areas: Real Case Study — The Persian Gulf.* Tech. Rept. 4. MoD Agreement NNR/2042/1. 42pp.

Lystad, S. and Tjelta, T. 1995. High Resolution Meteorological Grid for Clear Air Propagation Modelling in Northern Coastal Regions. *In: Propagation Assessment in Coastal Environment.* AGARD Conference Proceedings, vol. 567. Paper 41.

Mizzi, A. P. and Pielke, R. A. 1984. A Numerical Study of the Mesoscale Atmospheric Circulation Observed During a Coastal Upwelling Event on 23 August 1992. Part I: Sensitivity Studies. *Mon. Wea. Rev.*, **112**, 76–90.

Plant, R. S. and Atkinson, B. W. 1999. *Numerical Modelling of the Propagation Environment in the Atmospheric Boundary Layer of Littoral Areas — Resolution Effects.* Tech. Rept. 1. MoD Agreement FS2/2042/02. 61pp.

Plant, R. S. and Atkinson, B. W. 2000a. *Numerical Modelling of the Propagation Environment in the Atmospheric Boundary Layer of Littoral Areas — Horizontal Variations in the Marine Boundary Layer.* Tech. Rept. 2. MoD Agreement FS2/2042/02. 69pp.

Plant, R. S. and Atkinson, B. W. 2000b. *Numerical Modelling of the Propagation Environment in the Atmospheric Boundary Layer of Littoral Areas — Application of the TERPEM Propagation Model.* Tech. Rept. 3. MoD Agreement FS2/2042/02. 72pp.

Reed, R. J. and Lewis, R. M. 1980. Responses of Upper Ocean Temperatures to Diurnal and Synoptic–Scale Variations of Meteorological Parameters in the GATE B-scale Area. *Pages 99–127 of:* Siedler, G. and Woods, J. D. (eds), *GATE-1 Oceanography and Surface Layer Meteorology in the B/C Scale.* Supplement I to Deep Sea Research A, vol. 26.

Rogers, D. P., Johnson, D. W. and Friehe, C. A. 1995. The Stable Internal Boundary Layer Over a Cosatal Sea. Part I: Airborne Measurements of the Mean and Turbulence Structure. *J. Atmos Sci.*, **52**, 667–683.

Rogers, L. T. 1995. Effects of Spatial and Temporal Variability of Atmospheric Refractivity on the Accuracy of Propagation Assessments. *In: Propagation Assessment in Coastal Environment.* AGARD Conference Proceedings, vol. 567. Paper 31.

Skolink, M. I. 1980. *Introduction to Radar Systems.* McGraw Hill Book Company. 581pp.

Turton, J. D., Bennetts, D. A. and Farmer, S. F. G. 1988. An Introduction to Radio Ducting. *Meteorol. Mag.*, **117**, 245–254.

Wai, M. M.-K. 1988. Modelling the Effects of the Spatially Varying Sea Surface Temperature on the Marine Atmospheric Boundary Layer. *J. Atmos. Meteorol.*, **27**, 5–19.

Wai, M. M.-K. and Stage, S. A. 1989. Dynamical Analyses of Marine Atmospheric Boundary Layer Structure near the Gulf Stream Oceanic Front. *Quart. J. R. Meteorol. Soc.*, **115**, 29–44.

## Figure Captions

Fig. 1 Location of the SHAREM-115 area and the model domain. The boundaries are marked by solid and broken lines repectively.

Fig. 2 Domain used in the simulations, with the land area shaded. The simulated and observed environments at several points along the line through $y = -54\,\mathrm{km}$ are discussed in Sec. 4.3. Lines AB and CD are the location of the cross-sections discussed in Secs. 4.3.1 and 4.3.2 respectively.

Fig. 3 Initial conditions for Set 1 runs. (a) shows the potential temperature as a function of height. The mixing ratio is shown in (b).

Fig. 4 Initial conditions for Set 2 runs. (a) shows the potential temperature as a function of height. The mixing ratio is shown in (b).

Fig. 5 Initial conditions for Set 3 run with low winds. (a) shows the potential temperature as a function of height. The mixing ratio is shown in (b).

Fig. 6 Initial conditions for Set 3 run with high winds. (a) shows the potential temperature as a function of height. The mixing ratio is shown in (b).

Fig. 7 Sea surface temperature (SST) (°C) along the line $y = -54\,\mathrm{km}$ in the Set 4 low-wind run.

Fig. 8 Profiles for 1500LT along $y = -54\,\mathrm{km}$ at points $x = -120$ (land) and $x = 108\,\mathrm{km}$ (sea) of: (a) potential temperature (°C); (b) humidity ($\mathrm{g\,kg^{-1}}$); (c) modified refractivity ($M$-units). The data is obtained from the Set 1 simulation of the low-wind case.

Fig. 9 Profiles for 1500LT at the point $x = 210, y = -78\,\mathrm{km}$ of: (a) potential temperature (°C); (b) humidity ($\mathrm{g\,kg^{-1}}$); (c) modified refractivity ($M$-units). The data is obtained from the Set 1 simulation of the low-wind case.

Fig. 10 Profiles for 1200LT at the point $x = 210, y = -78\,\mathrm{km}$ of: (a) potential temperature (°C); (b) humidity ($\mathrm{g\,kg^{-1}}$); (c) modified refractivity ($M$-units). The data is obtained from the Set 1 simulation of the high-wind case.

Fig. 11 Profiles for 1400LT at the point $x = 210, y = -78\,\mathrm{km}$ of simulated and observed values of: (a) potential temperature (°C); (b) humidity ($\mathrm{g\,kg^{-1}}$); (c) modified refractivity ($M$-units). The simulation data is obtained from the Set 2 simulation of the low-wind case. The observations are for 1415–1425LT on 23 rd April 1996, taken in SHAREM-115 (Brooks *et al.*, 1997, Fig. 13).

Fig. 12 Profiles for 1300LT at the point $x = 186, y = -54\,\mathrm{km}$ of simulated and observed values of: (a) potential temperature (°C); (b) humidity ($\mathrm{g\,kg^{-1}}$); (c) modified refractivity ($M$-units). The simulation data is obtained from the Set 2 simulation of the high-wind case. The observations are for 1301–1307LT on 28 th April 1996, taken in SHAREM-115 (Brooks *et al.*, 1997, Fig. 24).

Fig. 13 Profiles for 1400 and 1800LT at the point $x = 210, y = -78\,\mathrm{km}$ of simulated and observed values of: (a) potential temperature (°C); (b) humidity ($\mathrm{g\,kg^{-1}}$); (c) modified refractivity ($M$-units). The simulation data is obtained from the Set 3 simulation of the low-wind case. The observations are for 1415–1425LT on 23 rd April 1996, taken in SHAREM-115 (Brooks *et al.*, 1997, Fig. 13).

Fig. 14 Profiles for 1300LT at the point $x = 186, y = -54\,\mathrm{km}$ of simulated and observed values of: (a) potential temperature (°C); (b) humidity ($\mathrm{g\,kg^{-1}}$); (c) modified refractivity ($M$-units). The simulation data is obtained from the Set 3 simulation of the high-wind case. The observations are for 1301–1307LT on 28 th April 1996, taken in SHAREM-115 (Brooks *et al.*, 1997, Fig. 24).

Fig. 15 Cross sections of vapour pressure (mb) along $y = -54\,\mathrm{km}$ in the low-wind run of Set 4. The upper plot is at 1200 hr, the middle at 1400 hr and the lower at 1600 hr.

Fig. 16 Cross sections of vapour pressure (mb) along $y = -54\,\mathrm{km}$ in the high-wind run of Set 4. The upper plot is at 1300 hr, the middle at 1400 hr and the lower at 1600 hr.

Fig. 17 Cross section of the wind at 1400 hr along $y = -54\,\mathrm{km}$ in the low-wind run of Set 4. The $u$ component is plotted in units of $\mathrm{ms^{-1}}$ and the $w$ component in units of $\mathrm{cms^{-1}}$. Scales are provided by a reference arrow shown at a height of 200 m and $x \sim 50\,\mathrm{km}$, representing $u = 7\,\mathrm{ms^{-1}}$ and $w = 7\,\mathrm{cms^{-1}}$.

Fig. 18 Cross-sections of potential temperature (°C) along line AB of Fig. 2 in the low-wind case of Set 3: (a) simulated values at 1400LT; (b) observations on 25 th April 1996, taken in SHAREM-115 (Brooks *et al.*, 1997, Fig. 32).

Fig. 19 Cross-sections of modified refractivity ($M$-units) along line AB of Fig. 2 in the low-wind case of Set 3: (a) simulated values at 1400LT; (b) observations on 25 th April 1996, taken in SHAREM-115 (Brooks *et al.*, 1997, Fig. 32).

Fig. 20 Cross-sections of potential temperature (°C) along line CD of Fig. 2 in the high-wind case of Set 3: (a) simulated values at 1400LT; (b)

observations on 28 th April 1996, taken in SHAREM-115 (Brooks *et al.*, 1997, Fig. 38).

Fig. 21 Cross-sections of modified refractivity ($M$-units) along line CD of Fig. 2 in the high-wind case of Set 3: (a) simulated values at 1400LT; (b) observations on 28 th April 1996, taken in SHAREM-115 (Brooks *et al.*, 1997, Fig. 38).

Fig.1 Location of SPAREM-115 area (- - - )and model domain ( — ).

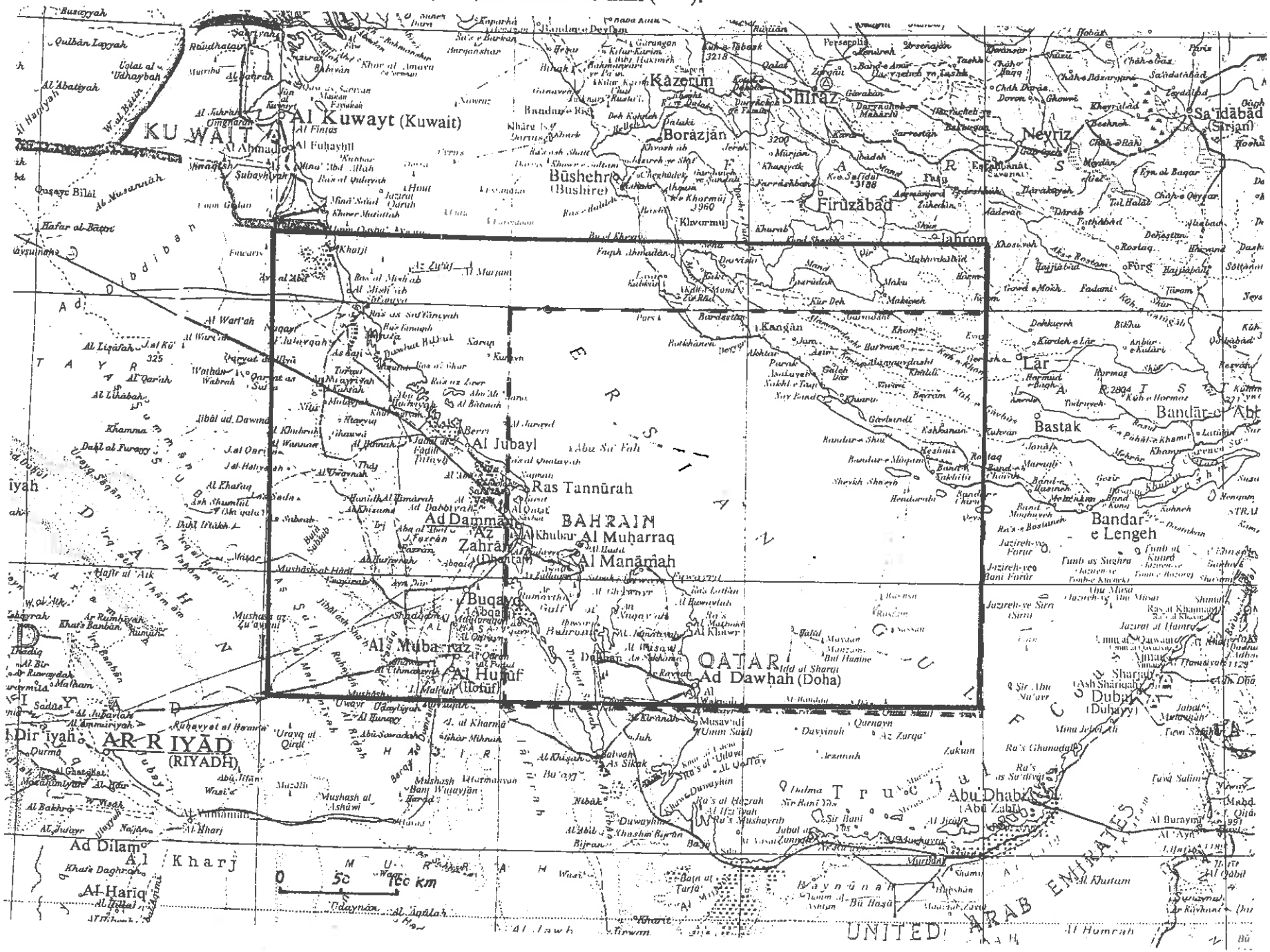

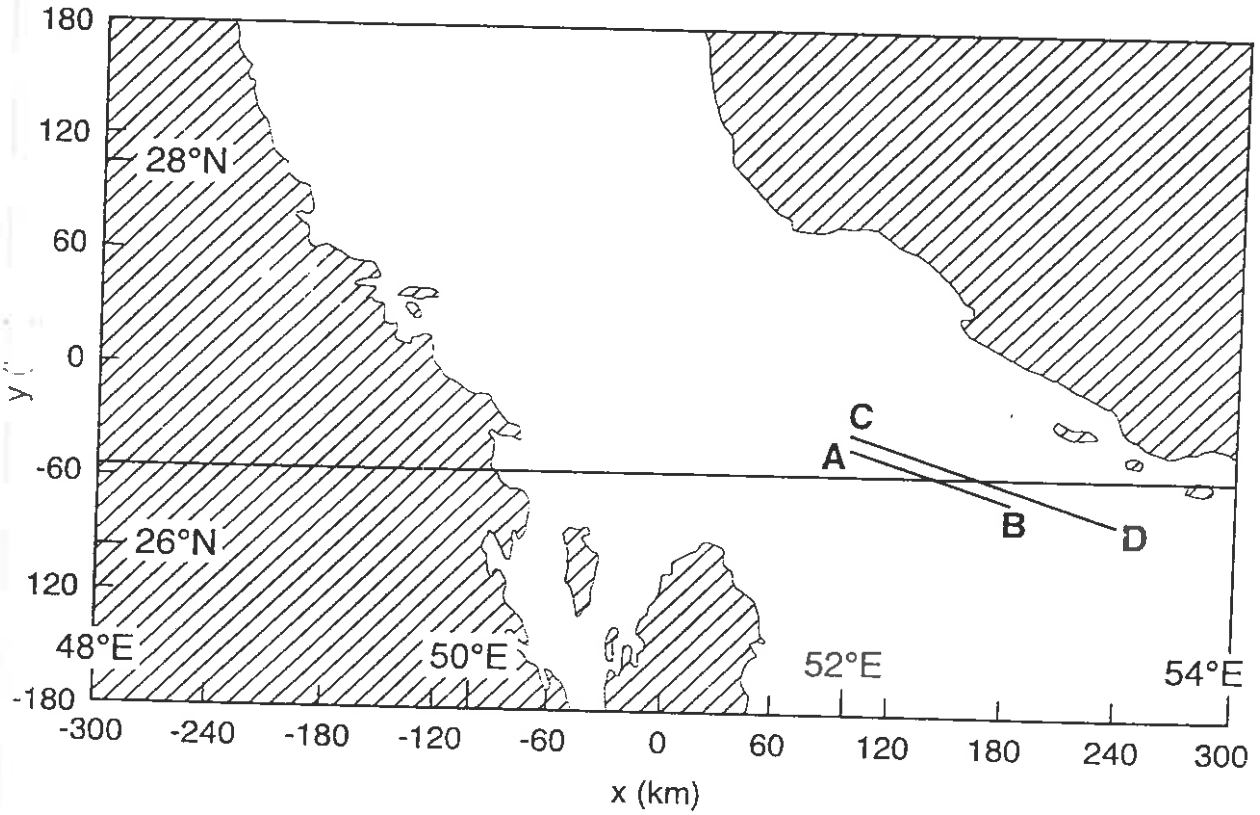
180
120
28°N
60
0
-60
26°N
120
48°E
50°E
52°E
54°E
-180
-300
-240
-180
-120
-60
0
60
120
180
240
300
x (km)
A
B
C
D

Figure 2.

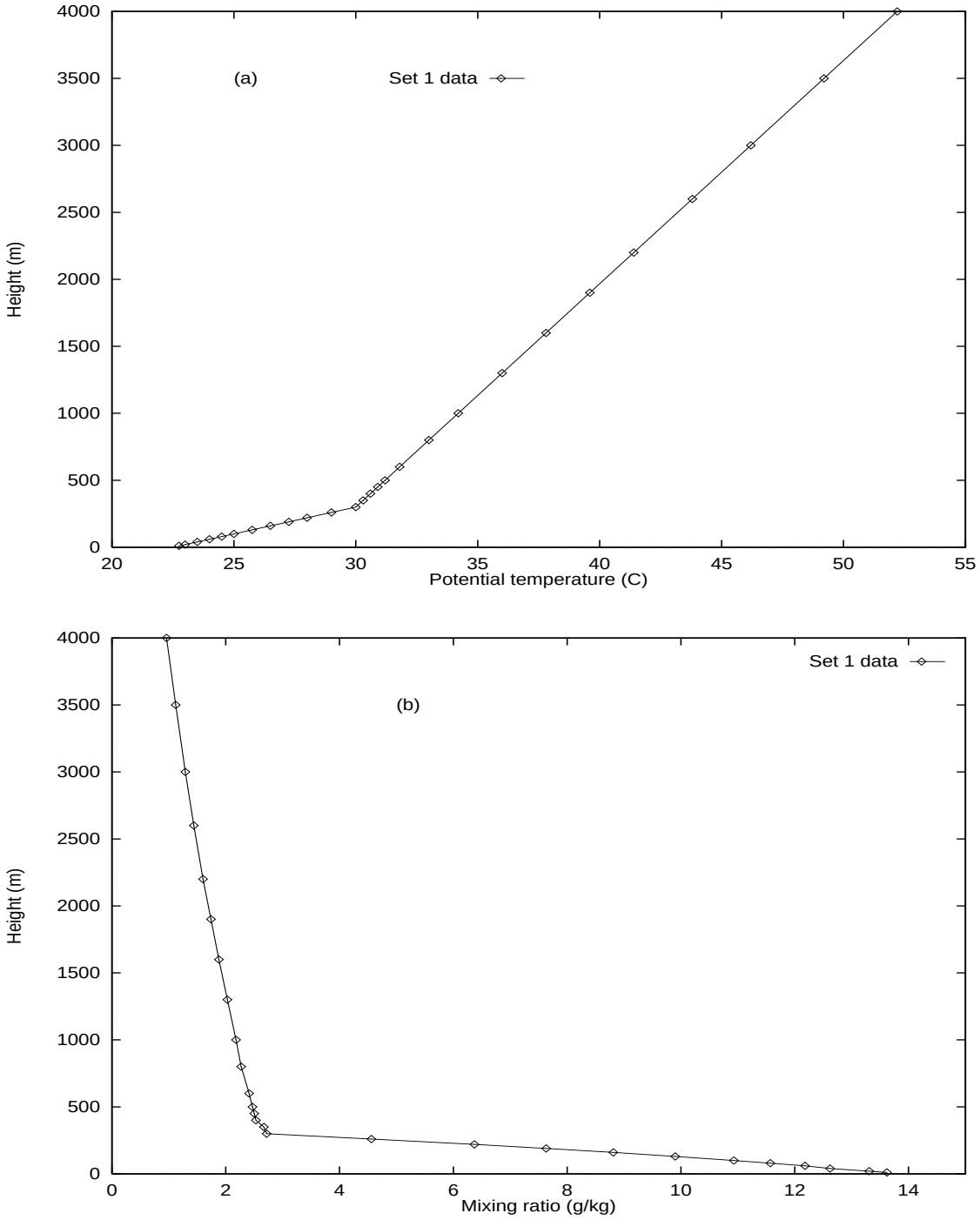


Figure 3: Initial conditions for Set 1 runs.

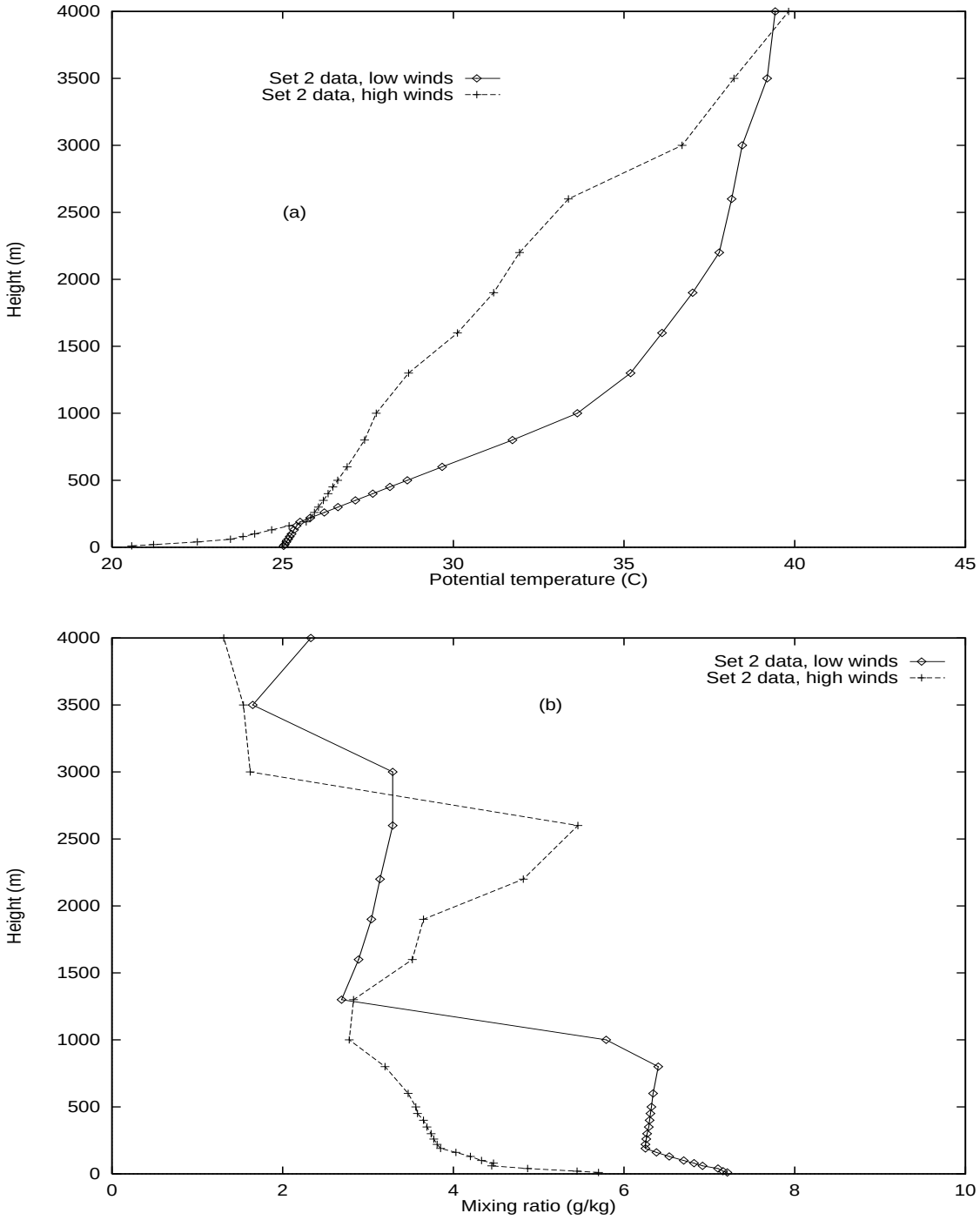


Figure 4: Initial conditions for Set 2 runs.

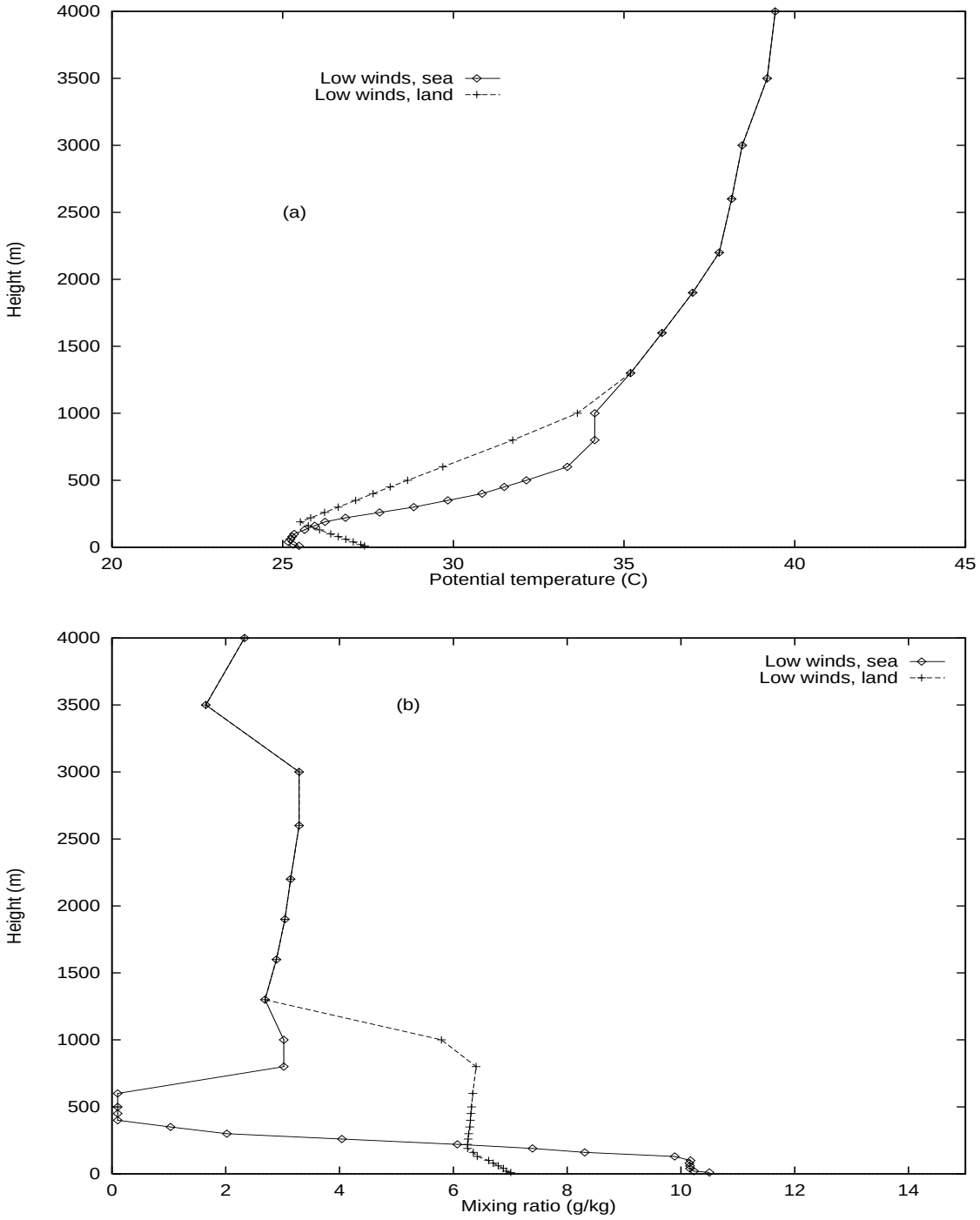


Figure 5: Initial conditions for the Set 3 run with low winds.

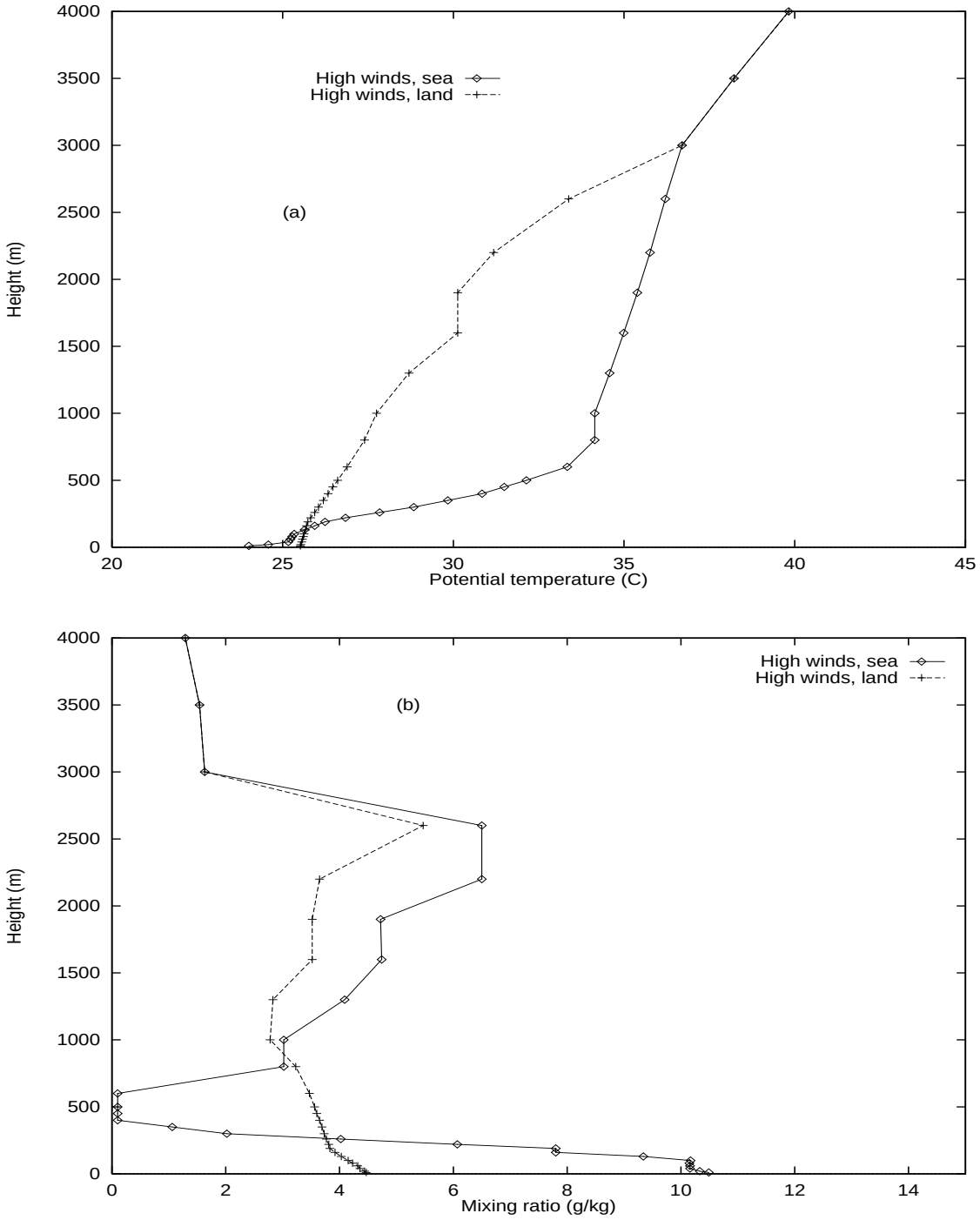


Figure 6: Initial conditions for the Set 3 run with high winds.

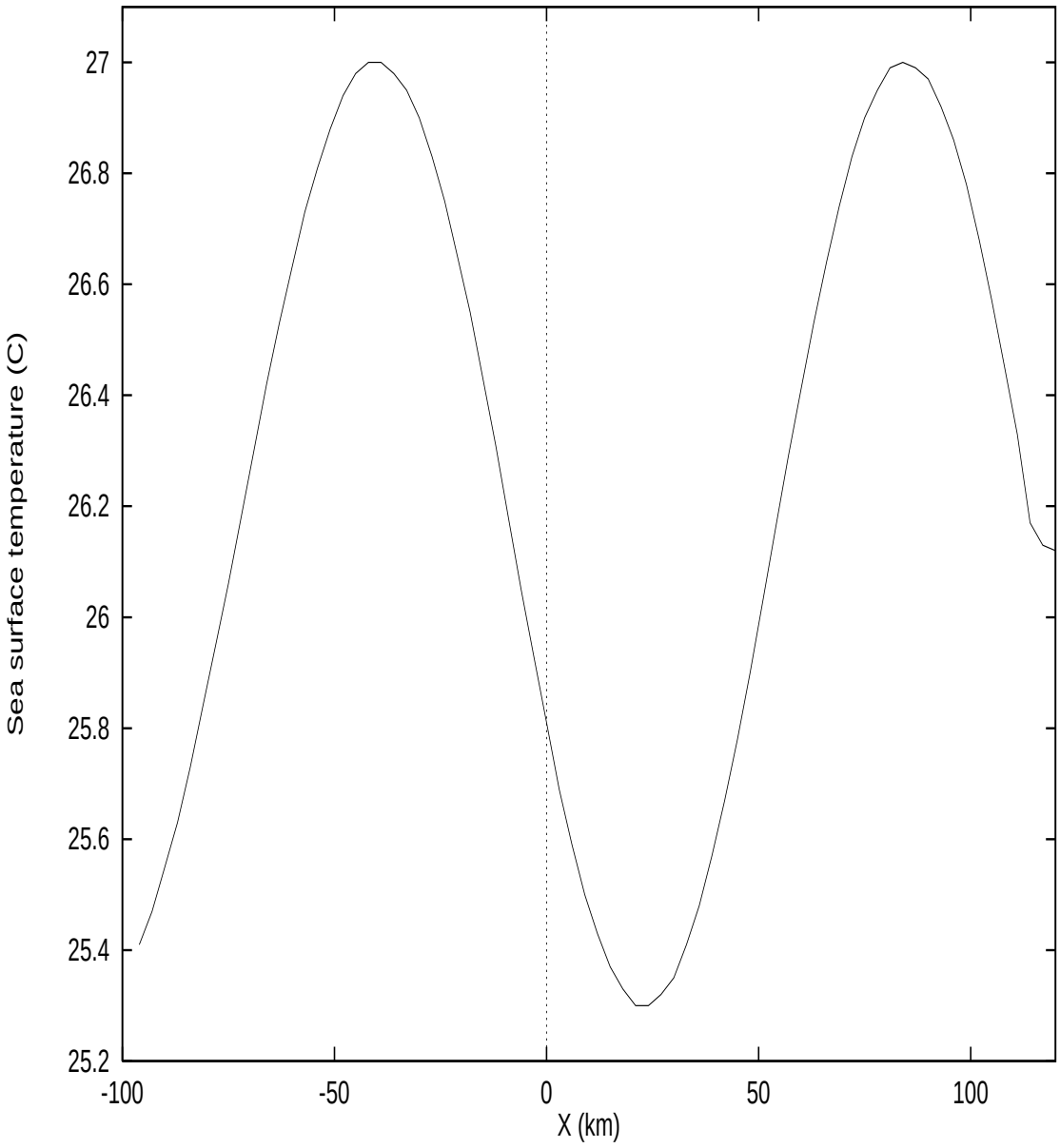


Figure 7: Sea surface temperature (SST) (°C) along the line $y = -54\,\mathrm{km}$ in the low wind run of Set 4.

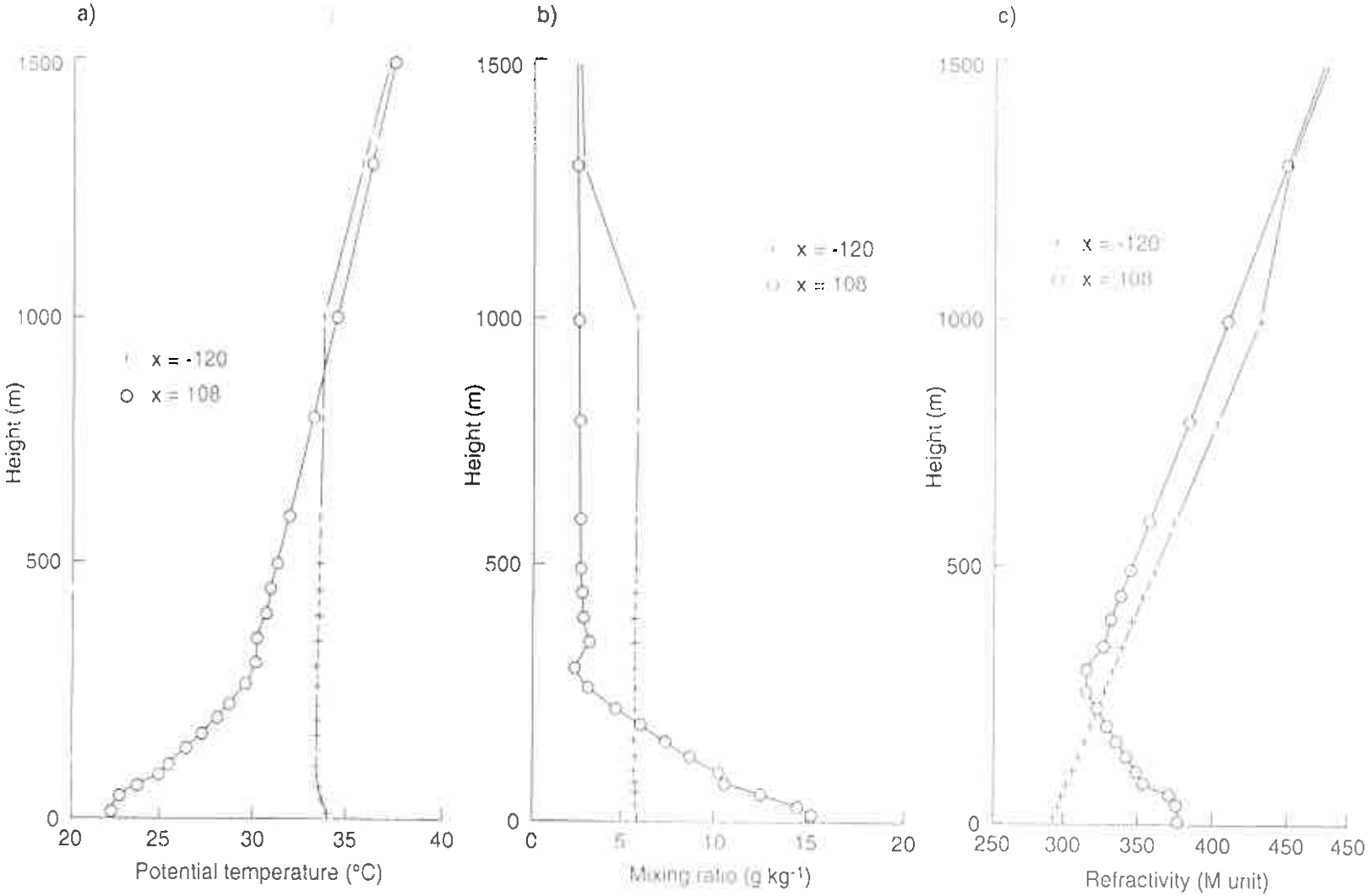
a)
b)
c)
1500
1000
500
0
Height (m)
x = -120
x = 108
20
25
30
35
40
Potential temperature (°C)
0
5
10
15
20
Mixing ratio (g kg-1)
250
300
350
400
450
Refractivity (M unit)

Figure 8.

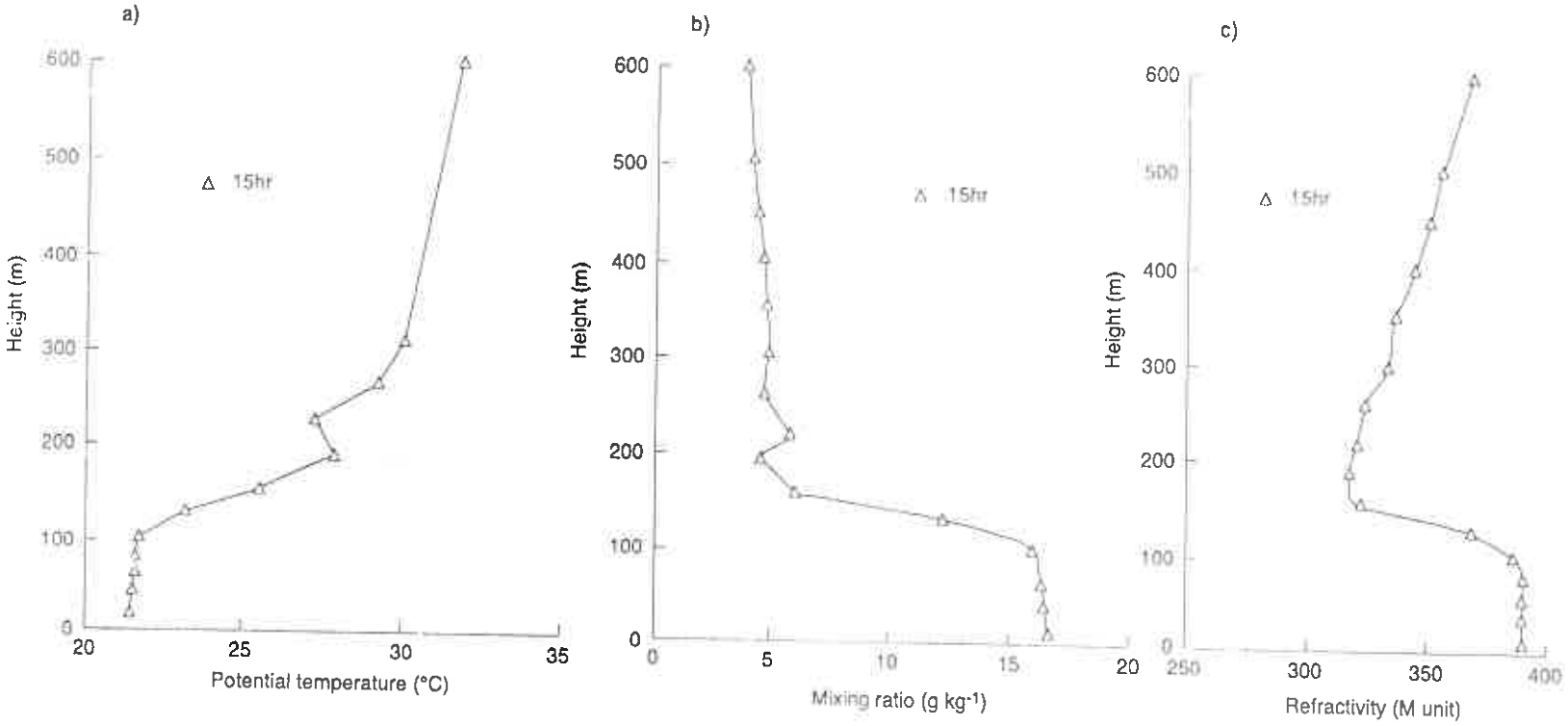
a)
b)
c)
Height (m)
600
500
400
300
200
100
0
△ 15hr
20
25
30
35
Potential temperature (°C)
0
5
10
15
20
Mixing ratio (g kg-1)
250
300
350
400
Refractivity (M unit)

Figure 9.

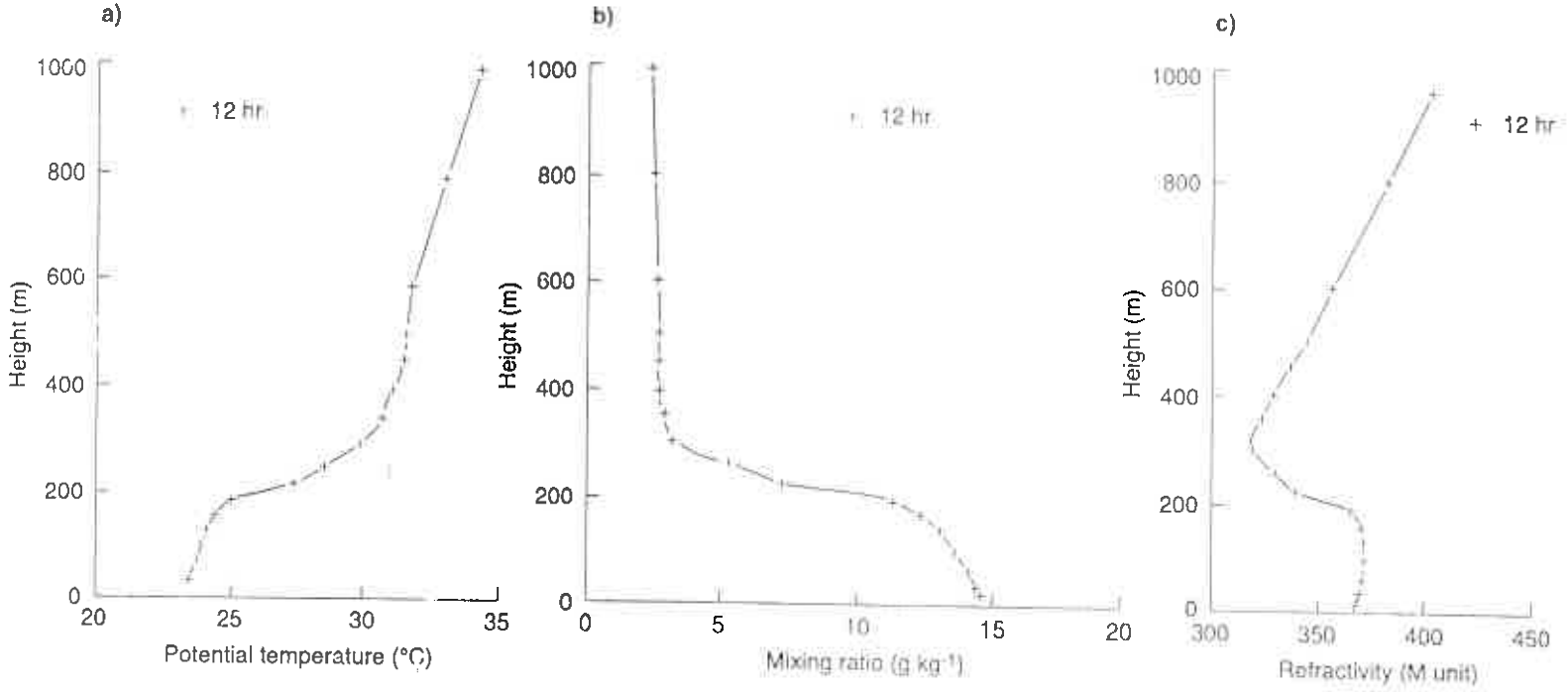
a)
b)
c)
1000
800
600
400
200
0
Height (m)
12 hr
20
25
30
35
Potential temperature (°C)
0
5
10
15
20
Mixing ratio (g kg⁻¹)
300
350
400
450
Refractivity (M unit)

Figure 10.

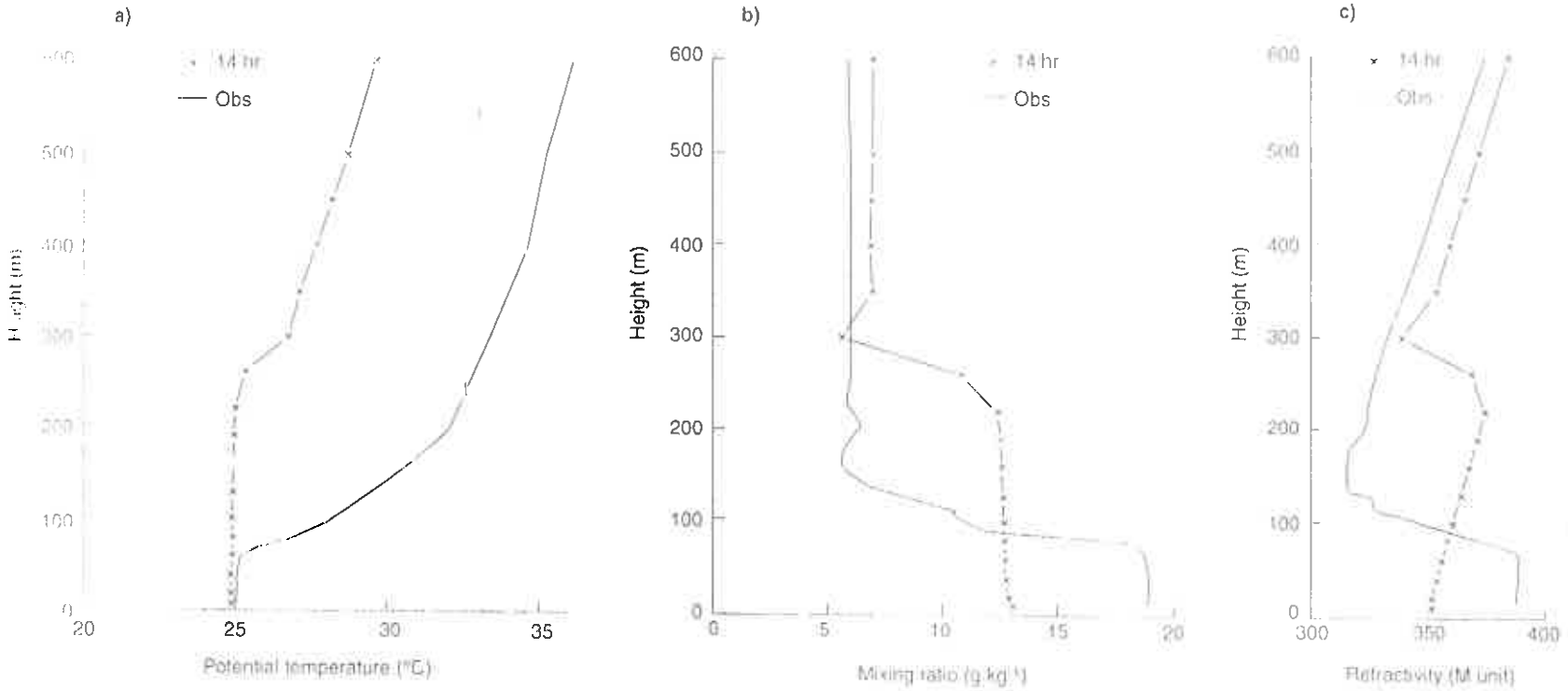
a)
14 hr
Obs
500
400
100
0
20
25
30
35
Potential temperature (°C)
b)
14 hr
Obs
600
500
400
300
200
100
0
Height (m)
0
5
10
15
20
c)
14 hr
Obs
600
500
400
300
200
100
0
Height (m)
300
350
400
Refractivity (M unit)

Figure 11.

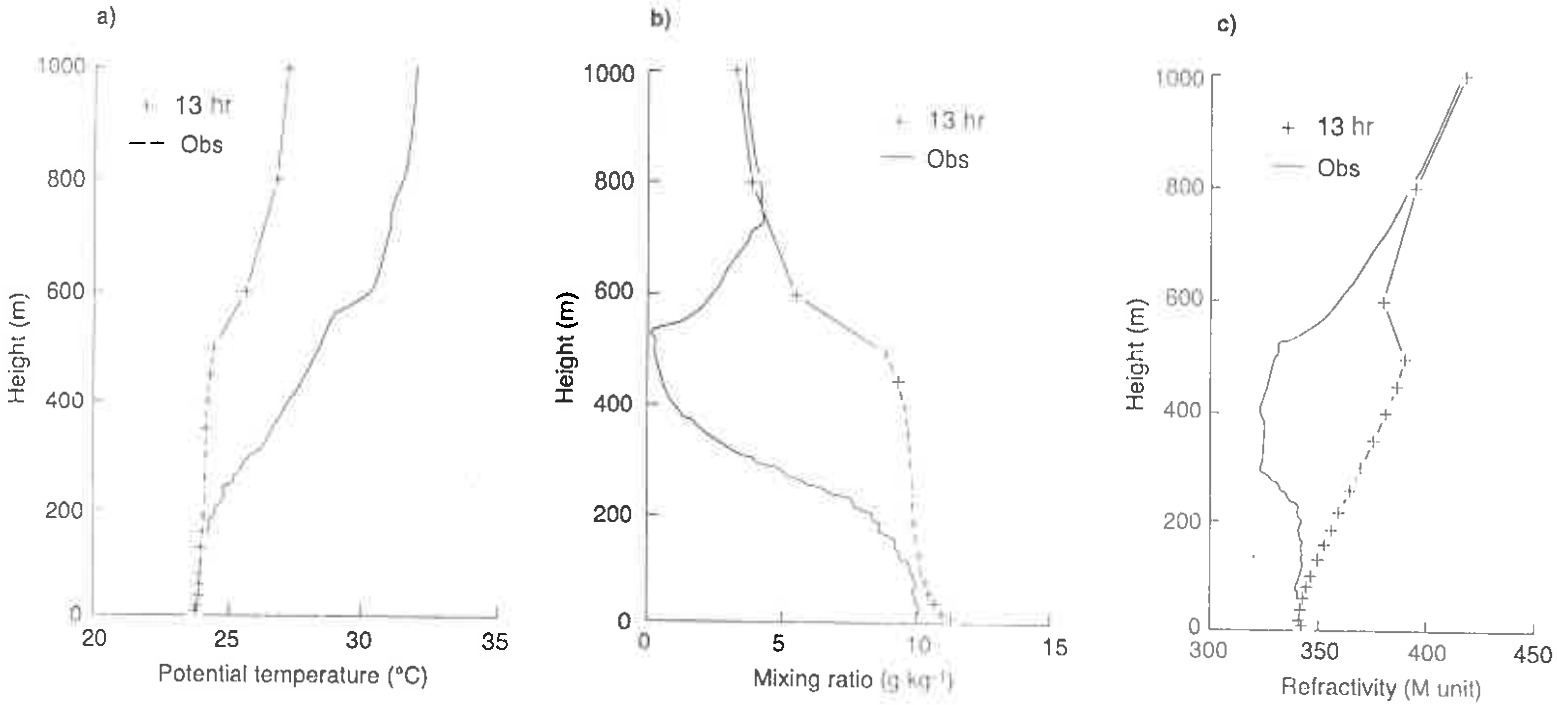
a)
b)
c)
13 hr
Obs
Height (m)
Potential temperature (°C)
Mixing ratio (g kg⁻¹)
Refractivity (M unit)
1000
800
600
400
200
0
20
25
30
35
5
10
15
300
350
400
450

Figure 12.

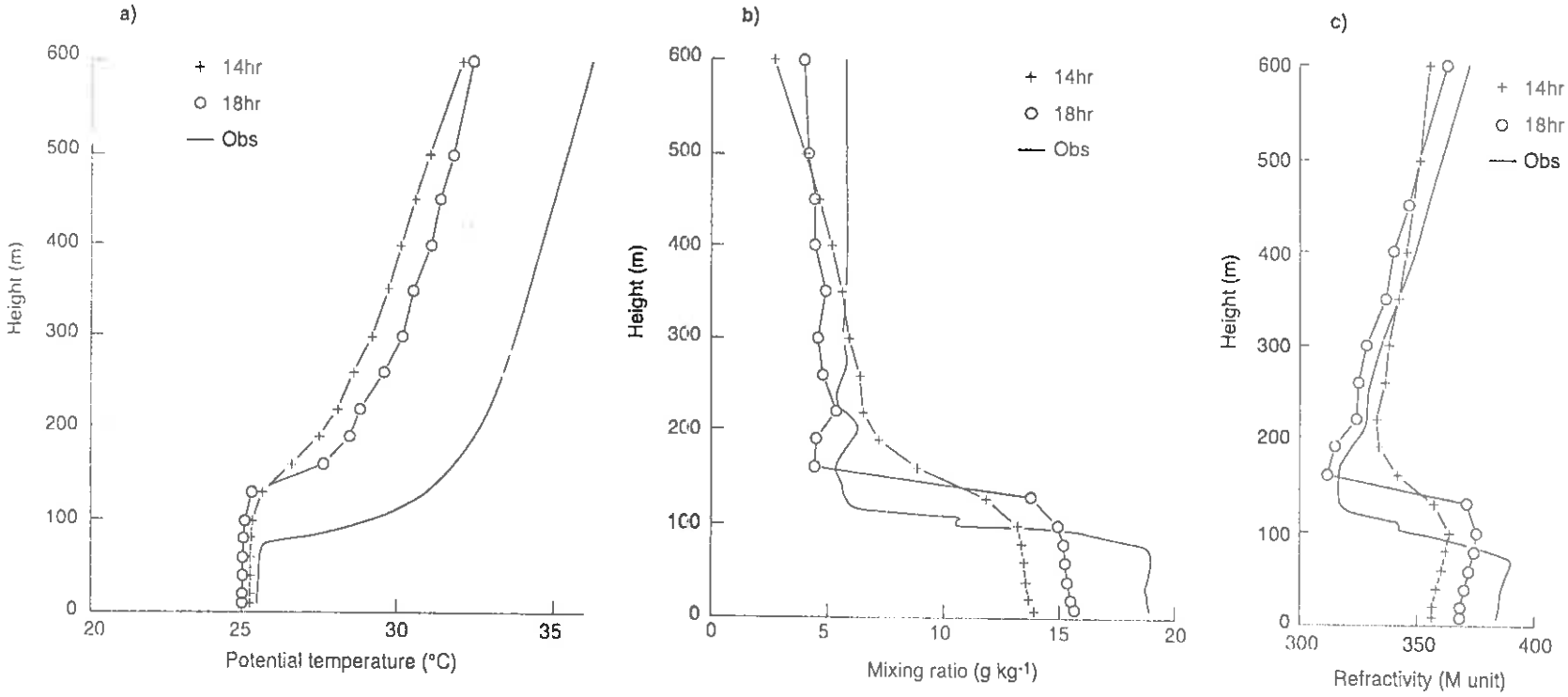
a)
b)
c)
14hr
18hr
Obs
Height (m)
Potential temperature (°C)
Mixing ratio (g kg-1)
Refractivity (M unit)

Figure 13.

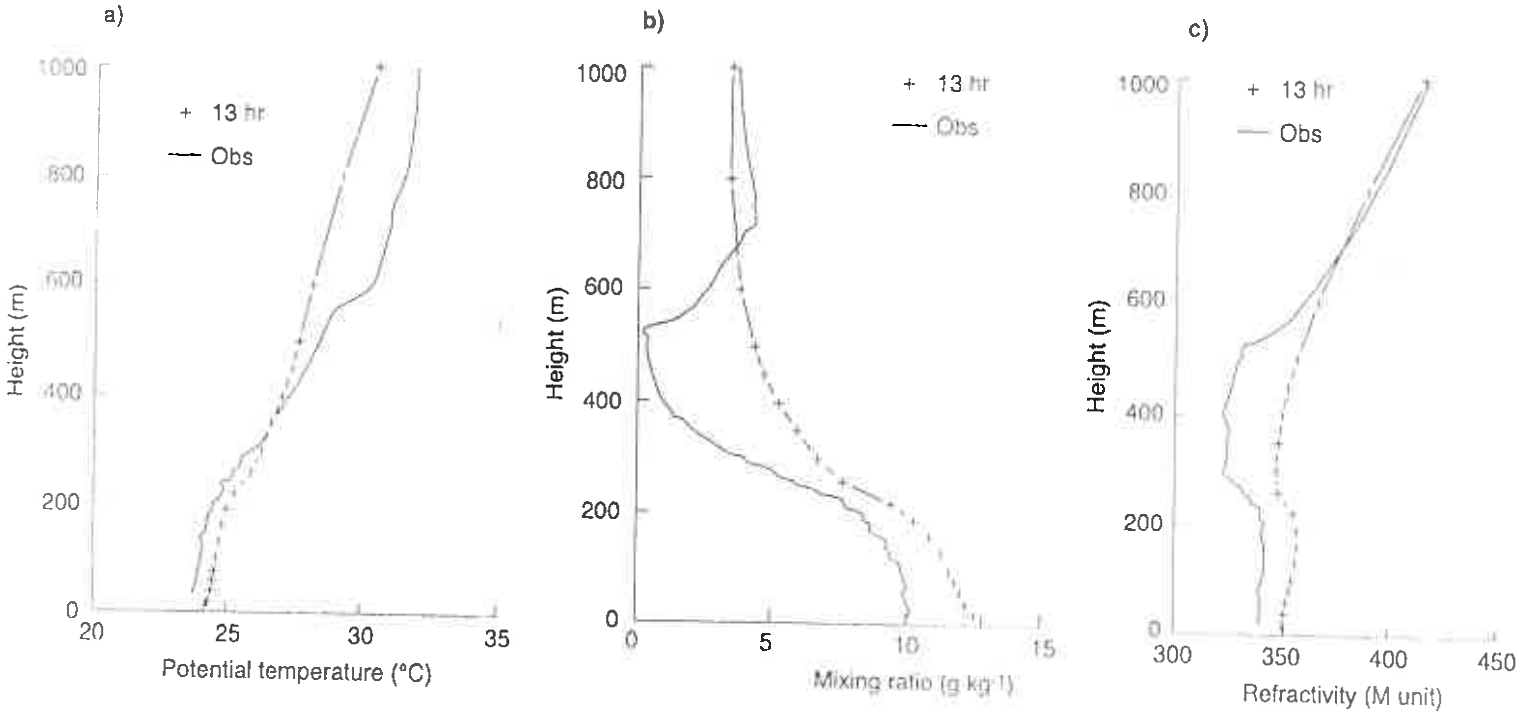
a)
b)
c)
+ 13 hr
Obs
Height (m)
1000
800
600
400
200
0
20
25
30
35
Potential temperature (°C)
0
5
10
15
Mixing ratio (g kg⁻¹)
300
350
400
450
Refractivity (M unit)

Figure 14.

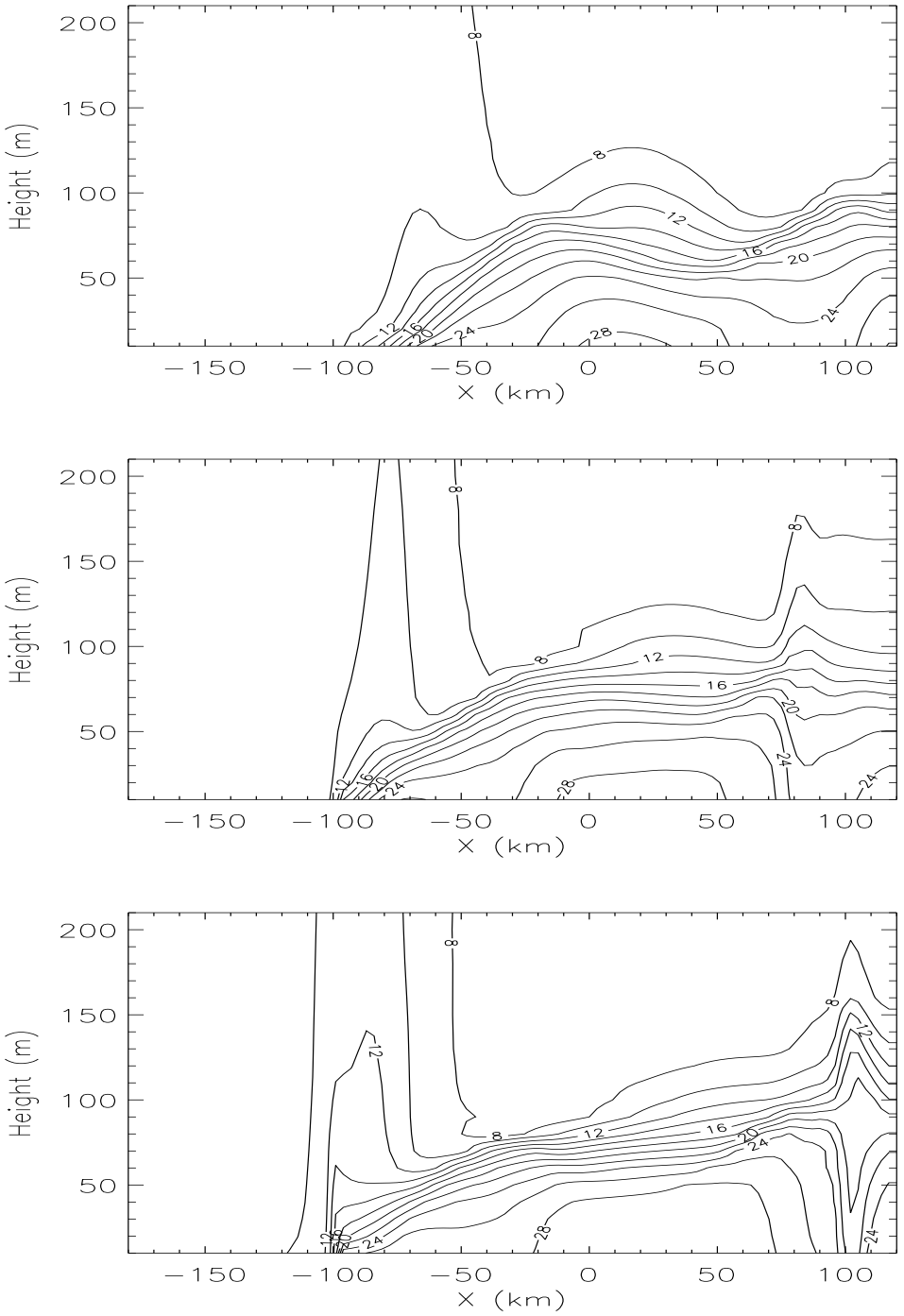


Figure 15: Cross sections of vapour pressure (mb) along $y = -54$ km in the low-wind run of Set 4. The upper plot is at 1200 hr, the middle at 1400 hr and the lower at 1600 hr.

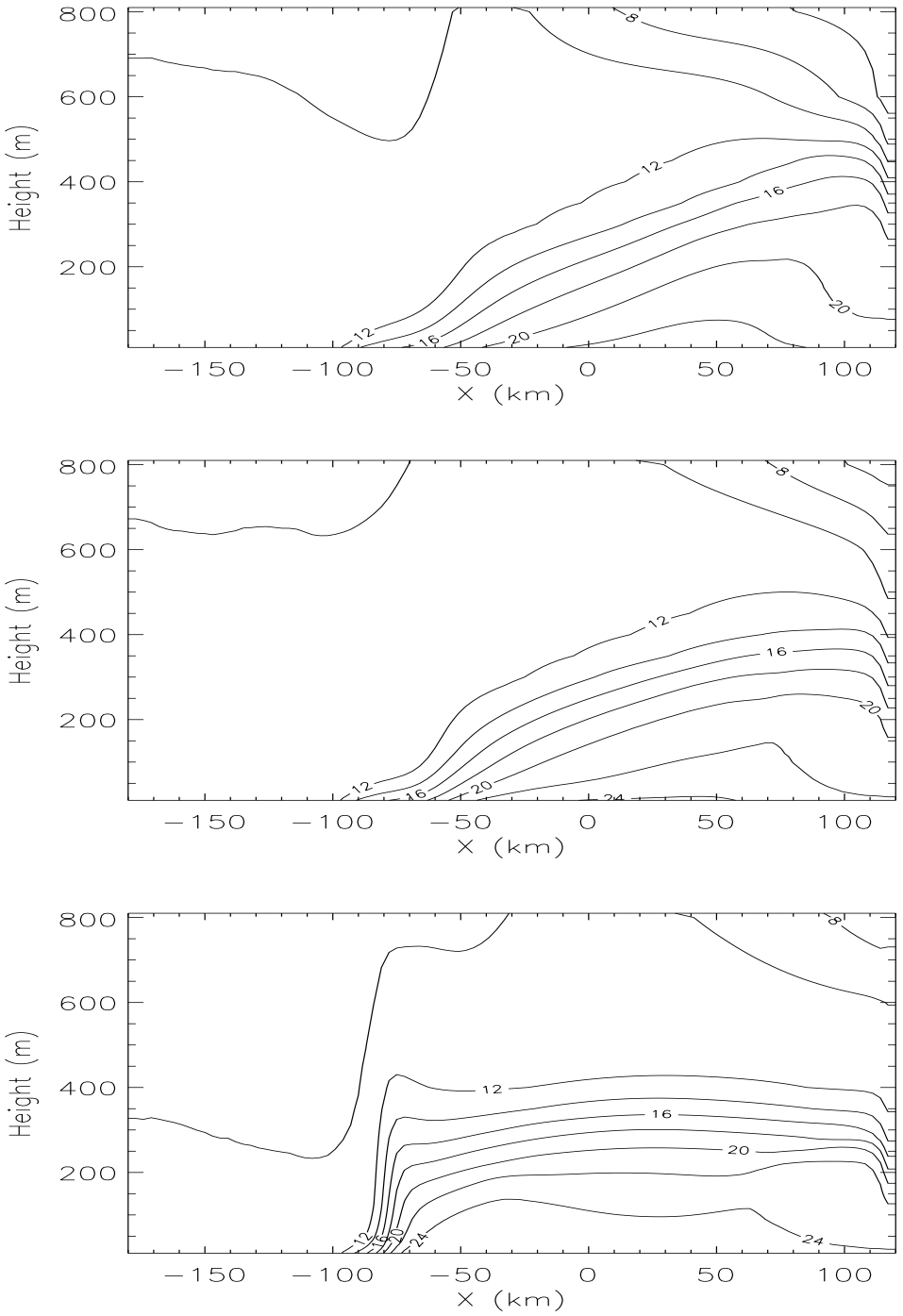


Figure 16: Cross sections of vapour pressure (mb) along $y = -54$ km in the high-wind run of Set 4. The upper plot is at 1300 hr, the middle at 1400 hr and the lower at 1600 hr.

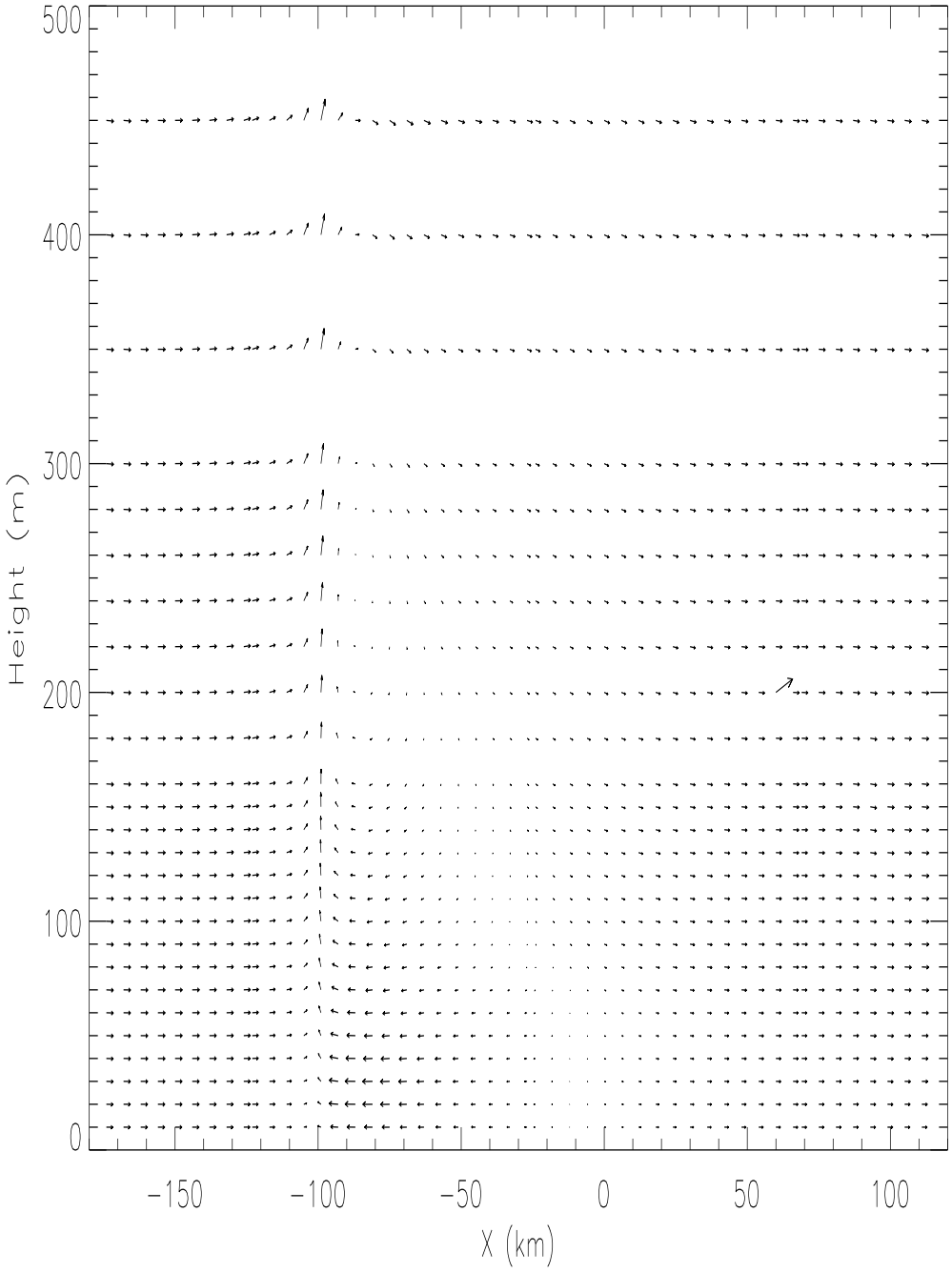


Figure 17: Cross section of the wind at 1400 hr along $y = -54\,\mathrm{km}$ in the low-wind run of Set 4. The $u$ component is plotted in units of $\mathrm{ms}^{-1}$ and the $w$ component in units of $\mathrm{cms}^{-1}$. Scales are provided by a reference arrow shown at a height of 200 m and $x \sim 50\,\mathrm{km}$, representing $u = 7\,\mathrm{ms}^{-1}$ and $w = 7\,\mathrm{cms}^{-1}$.